Inorganic Chemistry
including bioinorganic chemistry
October 6, 2014
Volume 53, Number 19
pubs.acs.org/IC

Iron-centered oxidation of a $Fe^{II}Mo^{VI}$ oxo cluster in four consecutive reversible steps

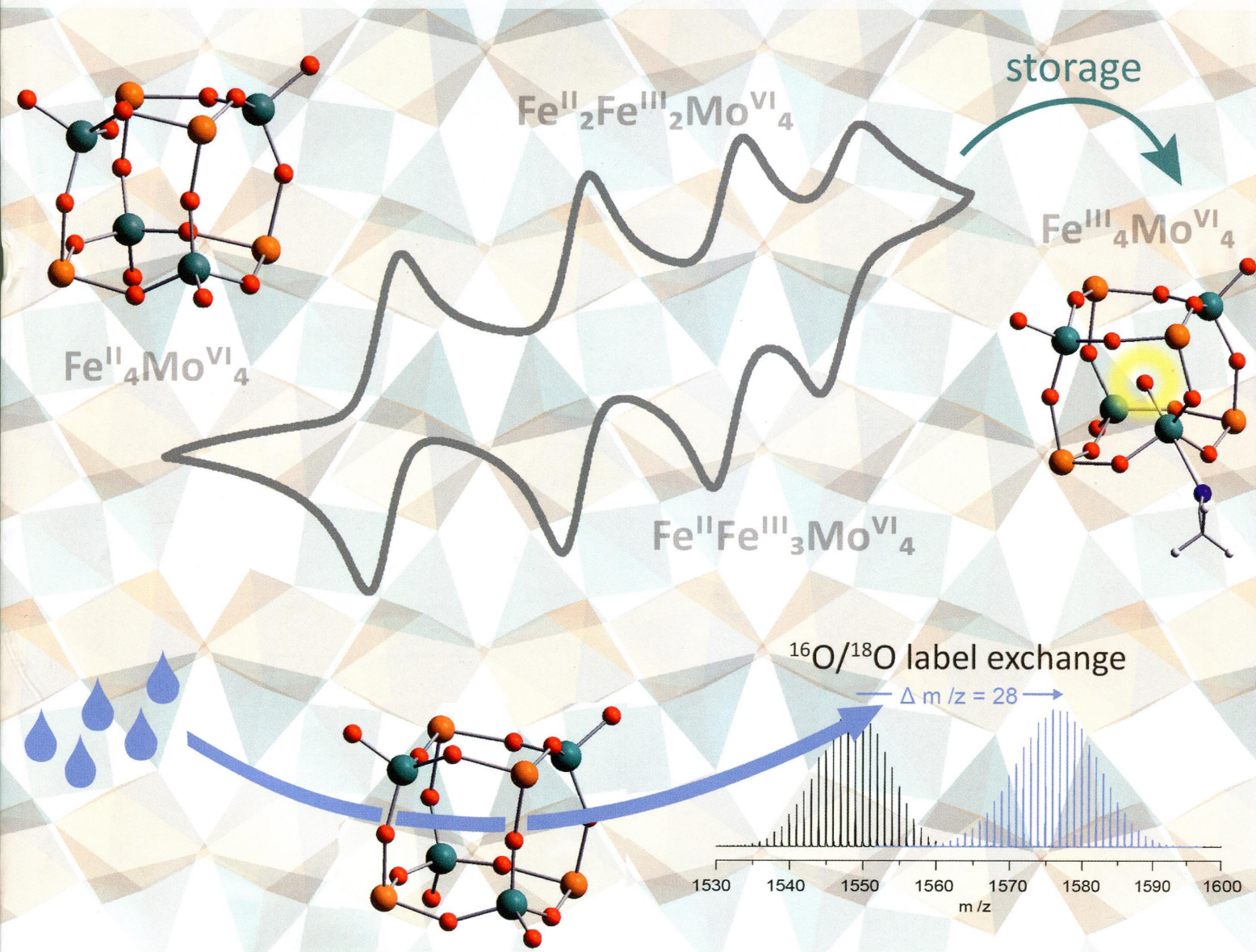

Inorganic Chemistry

OCTOBER 6, 2014
VOLUME 53 ISSUE 19

INOCAJ 53(19) 9983−10780 (2014)
ISSN 0020-1669
Registered in the U.S. Patent and Trademark Office

ON THE COVER: A distorted cubic framework, composed of alternating nitrogen-donor-ligated Fe^{2+} ions and $O{=}Mo^{4+}$ units linked by oxido ligands, can be oxidized in four reversible oxidation steps; after the final oxidation, one of the $O{=}Mo^{4+}$ corners experiences an unprecedented inversion, which places the respective terminal oxido ligand in the interior of the cage. The all-ferrous form exchanges all of its oxygen atoms with water, proving high anion mobility, which is similar to the behavior observed for industrially relevant ferric molybdates. This paper was inadvertently published in a previous issue. See J. P. Falkenhagen, B. Braun, E. Bill, D. Sattler, and C. Limberg *Inorg. Chem.* **2014**, *53* (14), 7294−7308.

Viewpoint

dx.doi.org/10.1021/ic500658x

Evaluation of Homogeneous Electrocatalysts by Cyclic Voltammetry
Eric S. Rountree, Brian D. McCarthy, Thomas T. Eisenhart, and Jillian L. Dempsey*

This Viewpoint details the use of cyclic voltammetry to evaluate molecular electrocatalysts. Beginning with the fundamentals of electrochemistry, cyclic voltammetry and practical experimental considerations for inorganic chemists are covered. In the second part, the application of cyclic voltammetry to characterize electrocatalysts is described in depth, and methods to extract figures of merit under ideal and nonideal conditions are highlighted.

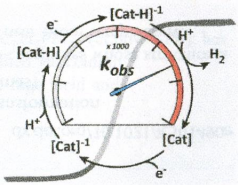

Communications

dx.doi.org/10.1021/ic5007764

Cisplatin Inhibits the Formation of a Reactive Intermediate during Copper-Catalyzed Oxidation of Amyloid β Peptide
Gulshan R. Walke, Srikanth Rapole, and Prasad P. Kulkarni*

The interaction of cisplatin with Aβ1-16 in the presence of Cu^{II} was investigated using cyclic voltammetry. The mass spectrometry data show complete inhibition of copper-catalyzed decarboxylation/deamination of the Asp1 residue of Aβ1-16 in the presence of cisplatin. Overall, a novel mode by which cisplatin inhibits copper-catalyzed oxidation of Aβ was reported. These findings may lead to the design of better platinum complexes to treat oxidative stress in Alzheimer's disease.

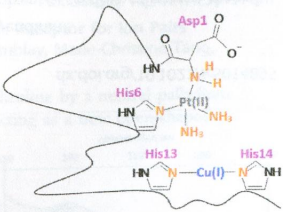

10006 Ⓢ dx.doi.org/10.1021/ic501062r

Why Does Enzyme Not Leach from Metal–Organic Frameworks (MOFs)? Unveiling the Interactions between an Enzyme Molecule and a MOF

Yao Chen, Sungyub Han, Xiao Li,* Zhenjie Zhang, and Shengqian Ma*

The strong interactions between microperoxidase (MP-11) and a metal–organic framework (MOF) have been identified to account for the retention of MP-11 molecules within the MOF pores, whereas the severe leaching of MP-11 from MCM-41 stems from the lack of specific interactions between enzyme molecule and the mesoporous silica material.

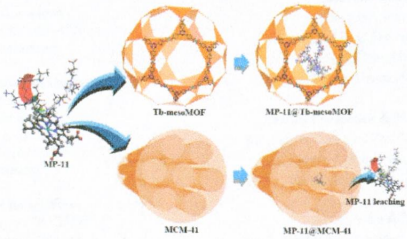

10009 Ⓢ dx.doi.org/10.1021/ic501195y

High-Temperature Spin Crossover in a Mononuclear Six-Coordinate Cobalt(II) Complex

Joanna Palion-Gazda, Anna Świtlicka-Olszewska, Barbara Machura,* Thais Grancha, Emilio Pardo, Francesc Lloret, and Miguel Julve*

The six-coordinate cobalt(II) complex of formula [Co(tppz)2](tcm)2 [tppz = 2,3,5,6-tetrakis(2-pyridyl)pyrazine and tcm = tricyanomethanide anion] exhibits a thermally induced spin-crossover behavior from a high spin ($S = {}^3/_2$) at higher temperatures to a low spin ($S = {}^1/_2$) at lower temperatures, with the low-spin phase being achieved at $T \leq 200$ K.

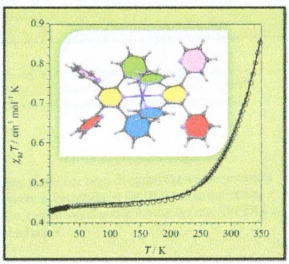

10012 Ⓢ dx.doi.org/10.1021/ic501290q

The Presence of Fast-Exchanging Proton Species in Aqueous Solutions of paraCEST Agents Can Impact Rate Constants Measured for Slower Exchanging Species When Fitting CEST Spectra to the Bloch Equations

Osasere M. Evbuomwan,* Joohwan Lee, Mark Woods, and A. Dean Sherry*

Mixtures containing varying proportions of two complexes with different SAP and TSAP isomer populations were prepared, and the water-exchange rate constant of the SAP isomer was determined using the Bloch equations and the omega plot method. The results show that the presence of the TSAP isomer resulted in a significant overestimation of the water-exchange rate constants of the SAP isomer when the CEST data are fitted to the Bloch equations.

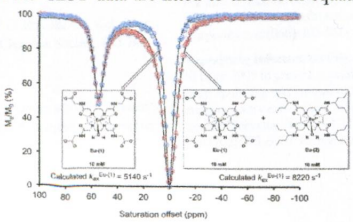

10015 S

dx.doi.org/10.1021/ic501337c

Selective Binding and Reverse Transcription Inhibition of Single-Strand poly(A) RNA by Metal TMPyP Complexes

Zhu-Xin Zhou, Feng Gao,* Xing Chen, Xiang-Jing Tian, and Liang-Nian Ji

Ni-, Cu-, and Zn-TMPyP are capable of binding to single-strand poly(A) RNA with high preference and affinity and inhibiting the reverse transcription of RNA by both M-MuLV and HIV-1 reverse transcriptase. With 10 nM azidothymidine, the IC_{50} value of M-TMPyP could be lowered to 10^{-1} μM order.

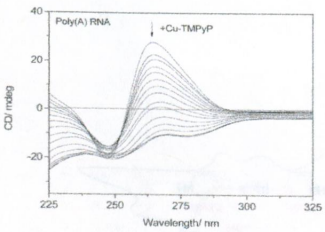

10018 S

dx.doi.org/10.1021/ic5014895

Spheroid Metallocavitands with Eight Calixarene-Shaped Receptors on the Surface

Bhaskaran Shankar, Palani Elumalai, Shankar Deval Sathiyashivan, and Malaichamy Sathiyendiran*

Neutral and heteroleptic rhenium(I)-based spheroid metallocavitands possessing eight solvent-accessible calixarene-shaped receptors on the surface were assembled in a one-step process.

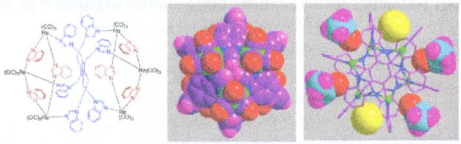

10021 S

dx.doi.org/10.1021/ic501490e

Formation of Heterobimetallic Zirconium/Cobalt Diimido Complexes via a Four-Electron Transformation

Bing Wu, Raúl Hernández Sánchez, Mark W. Bezpalko, Bruce M. Foxman, and Christine M. Thomas*

Four-electron oxidative nitrene transfer to reduced zirconium/cobalt complexes affords diimido complexes whose structure is dictated by imido substituents. A bridged imido complex is shown to undergo spin crossover near room temperature.

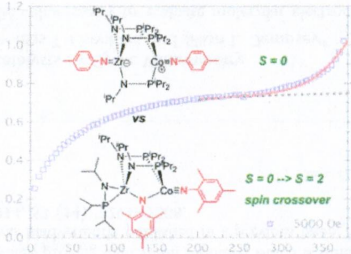

10024 S dx.doi.org/10.1021/ic501492c

Indium Metal–Organic Frameworks as High-Performance Heterogeneous Catalysts for the Synthesis of Amino Acid Derivatives

Jing Xia, Jianing Xu, Yong Fan, Tianyou Song, Li Wang,* and Jifu Zheng*

Microporous In-MOF **2** as a heterogeneous Lewis acid–base bifunctional catalyst can catalyze the Strecker reaction, affording the corresponding α-aminonitriles in good-to-excellent yield. It also catalyzes the Mannich reaction to give the corresponding β-amino esters in high conversion yield.

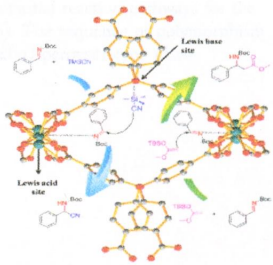

10027 S dx.doi.org/10.1021/ic501556w

Zeolitic Metal–Organic Frameworks Based on Amino Acid

E Yang, Lin Wang, Fei Wang,* Qipu Lin, Yao Kang, and Jian Zhang*

Two enantiomorphic metal–organic frameworks with zeotype SOD topology have been successfully synthesized from enantiopure L-alanine and D-alanine, respectively.

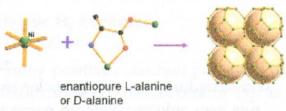

10030 S dx.doi.org/10.1021/ic5017164

Photoactive Ru(II) Complexes With Dioxinophenanthroline Ligands Are Potent Cytotoxic Agents

Achmad N. Hidayatullah, Erin Wachter, David K. Heidary, Sean Parkin, and Edith C. Glazer*

The effect of distortion on the phototoxicity index (PI) was explored for light-activated Ru(II) polypyridyl complexes containing a nonplanar dioxinophenanthroline (dop) ligand. The most distorted complex undergoes rapid photoinduced ligand loss and was found to be the most potent, with a 1880-fold increase in cytotoxicity in cancer cells. The compound was also found to be 19 times more potent than cisplatin, a commonly used chemotherapeutic agent, demonstrating a design principle for optimizing the PI.

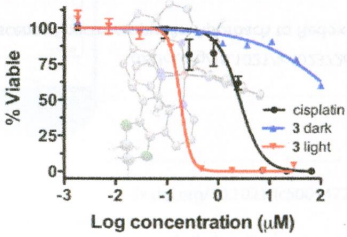

10033 S dx.doi.org/10.1021/ic501787m

Redox-Induced Change in the Ligand Coordination Mode

Victor Ovcharenko,* Olga Kuznetsova, Elena Fursova, Galina Romanenko, Alexey Polushkin, and Renad Sagdeev

The reaction of cobalt(II) pivalate with a spin-labeled Schiff base (HL^1) formed trinuclear complex $[Co_3(Piv)_2L^1{}_2L^2{}_2]$ containing both nitroxide L^1 and the product of its single-electron reduction, nitrone L^2. A reduction of L^1 to L^2 led to a change in the set of donor atoms and even in the size of the metallocycle.

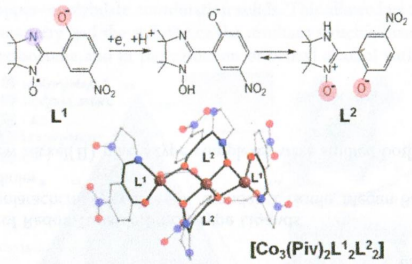

10036 S dx.doi.org/10.1021/ic5019345

Synthesis and Characterization of a New Binucleating Tetraphosphine Ligand Based on 1,2-Phenylene Chelates and the Structures of Dinickel Tetrachloride Complexes of the Ligand

William J. Schreiter, Alexandre R. Monteil, Ekaterina Kalachnikova, Marc A. Peterson, Marshall D. Moulis, Ciera D. Gasery, Gregory T. McCandless, Frank R. Fronczek, and George G. Stanley*

A new binucleating tetraphosphine ligand, *rac*- and *meso*-$(Et_2P\text{-}1,2\text{-}C_6H_4)P(Ph)CH_2(Ph)P(1,2\text{-}C_6H_4PEt_2)$ (et,ph-P4-Ph), has been synthesized. Separation and purification of the ligand diastereomers have been accomplished via column chromatography. Ni_2Cl_4(et,ph-P4-Ph) complexes of both diastereomers have been prepared in high yield and crystallographically characterized.

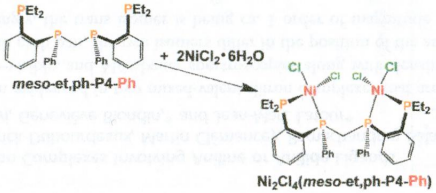

10039 S dx.doi.org/10.1021/ic501970m

Palladium(II)-Directed Self-Assembly of a Neutral Molecular Triangle as a Heteroditopic Receptor for Ion Pairs

Marie-Pierre Santoni, Amlan K. Pal, Daniel Chartrand, Garry S. Hanan,* Pierre Ménard-Tremblay, Marie-Christine Tang, Karine Venne, Alexandra Furtos, and Bernold Hasenknopf*

A new neutral and triangular metallocavitand, based on the self-assembly of 4,7-phenanthroline by a neutral palladium complex, has demonstrated the capacity to host both anionic and cationic guests, thus acting as a new open-shaped heteroditopic receptor.

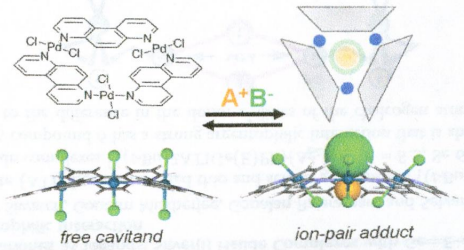

10042 dx.doi.org/10.1021/ic5020048

Advances in Understanding the Mechanism and Improved Stability of the Synthesis of Ammonia from Air and Water in Hydroxide Suspensions of Nanoscale Fe_2O_3

Fang-Fang Li and Stuart Licht*

We report a new understanding of the mechanism of STEP NH_3 production via an iron intermediate in which H_2 and NH_3 are cogenerated by different electron-transfer pathways. Enhancements are presented for this CO_2-free synthesis, which uses suspensions of nano-Fe_2O_3 in high-temperature hydroxide electrolytes at nickel and Monel electrodes, and the Coulombic efficiency of NH_3 conversion reaches as high as 71%. Solar thermal can contribute to the energy to drive this synthesis (STEP NH_3).

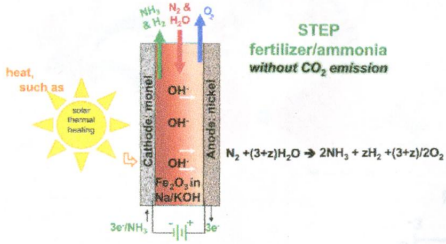

Articles

10045 dx.doi.org/10.1021/ic402372c

Direct Observation of Bis(dicarbollyl)nickel Conformers in Solution by Fluorescence Spectroscopy: An Approach to Redox-Controlled Metallacarborane Molecular Motors

Alexander V. Safronov, Natalia I. Shlyakhtina, Thomas A. Everett, Monika R. VanGordon, Yulia V. Sevryugina, Satish S. Jalisatgi, and M. Frederick Hawthorne*

The solution structures of substituted bis(dicarbollyl)nickel complexes in Ni^{III} and Ni^{IV} oxidation states were investigated by fluorescence spectroscopy. Symmetrically positioned pyrene molecules served as fluorescent probes to enable the observation of meso-trans/*dl*-gauche and *dl*-cis/*dl*-gauche cage conformations for nickelacarboranes in the Ni^{III} and Ni^{IV} oxidation states, respectively. The absence of the energetically disfavored conformers was demonstrated based on spectroscopic data and conformer energy calculations in solution. Conformational persistence indicates that bis(dicarbollyl)nickel complexes may provide templates for building electrically driven and/or photodriven molecular motors.

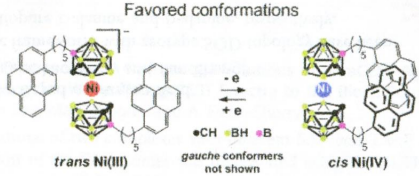

10054 dx.doi.org/10.1021/ic5008389

Use of Thio and Seleno Germanones as Ligands: Silver(I) Halide Complexes with Ge=E→Ag−I (E = S, Se) Moieties and Chalcogen-Dependent Argentophilic Interaction

Dhirendra Yadav, Rahul Kumar Siwatch, Goutam Mukherjee, Gopalan Rajaraman, and Selvarajan Nagendran*

Reaction of aminotroponiminate (ATI) ligand stabilized thio and seleno germanones [(*t*-Bu)2ATIGe(E)Ph] (E = S **3**, Se **4**) with AgI afforded silver(I) iodide complexes [{(*t*-Bu)2ATIGe(E)Ph}(Ag_2I_2)] (E = S **5**, Se **6**) with hitherto unknown Ge=E → Ag−I moieties. Interestingly, compound **6** has a strong argentophilic interaction that is absent in compound **5**. Theoretical studies reveals that this is due to the difference in the donor abilities of the chalcogen atoms.

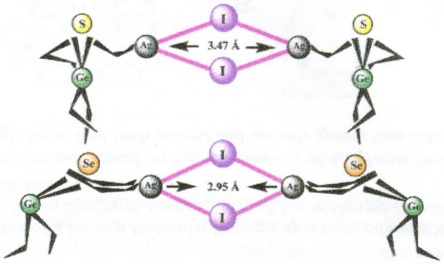

10060 dx.doi.org/10.1021/ic501793v

Cis/Trans Isomerizations in Diiron Complexes Involving Aniline or Anilide Ligands

Eric Gouré, Michaël Carboni, Patrick Dubourdeaux, Martin Clémancey, Ramachandran Balasubramanian, Colette Lebrun, Pierre-Alain Bayle, Pascale Maldivi, Geneviève Blondin,* and Jean-Marc Latour*

Isomerization reactions have been evidenced in two mixed-valent diiron complexes that are related by the (de)protonation of an aniline ligand. ^{1}H NMR, UV−visible, and Mössbauer spectroscopies along with density functional theory calculations converged to conclude that, within each pair, the two isomers differ in the position of the aniline/anilide ligand with respect to the bridging phenoxide. Interestingly, the trans isomer is being ca. 1 order of magnitude more acidic than the cis isomer.

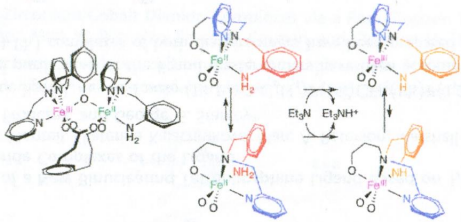

10070 dx.doi.org/10.1021/ic500657e

Homoleptic Nickel(II) Complexes of Redox-Tunable Pincer-type Ligands

Jeewantha S. Hewage, Sarath Wanniarachchi, Tyler J. Morin, Brendan J. Liddle, Megan Banaszynski, Sergey V. Lindeman, Brian Bennett,* and James R. Gardinier*

The electronic properties of 12 new nickel(II) pincer-type complexes were studied both experimentally and computationally.

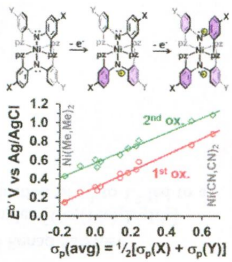

10085 Ⓢ dx.doi.org/10.1021/ic501270k

Studies on Polymorphic Sequence during the Formation of the 1:1 Ordered Perovskite-Type $BaCa_{0.335}M_{0.165}Nb_{0.5}O_{3-\delta}$ (M = Mn, Fe, Co) Using in Situ and ex Situ Powder X-ray Diffraction

Wang Hay Kan, Joey Lussier, Mario Bieringer, and Venkataraman Thangadurai*

Using in situ powder X-ray diffraction and electron diffraction, we have proposed the potential reaction pathways for the formation of the 1:1 ordered perovskite-type $BaCa_{0.335}M_{0.165}Nb_{0.5}O_{3-\delta}$ (M = Mn, Fe, Co). The sequence of polymorphism seems to follow simple cubic ($Pm\bar{3}m$), 1:2 ordered phase ($P\bar{3}m1$), and 1:1 ordered ($Fm\bar{3}m$) perovsite-type phase.

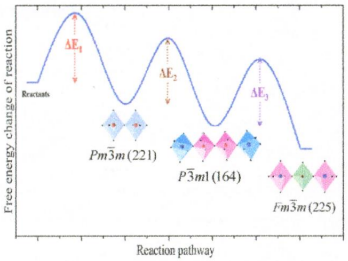

10094 Ⓢ dx.doi.org/10.1021/ic500840e

Electronic Effects on a Mononuclear Co Complex with a Pentadentate Ligand for Catalytic H_2 Evolution

Manohar Vennampalli, Guangchao Liang, Lakshmi Katta, Charles Edwin Webster,* and Xuan Zhao*

The replacement of pyridyls with isoquinoline groups in a pentadentate ligand results in more positive reduction potentials of Co centers, lower overpotential, higher turnover frequency, and enhanced stability for electrocatalytic production of H_2, as well as higher activity for photocatalytic H_2 evolution in neutral aqueous solution.

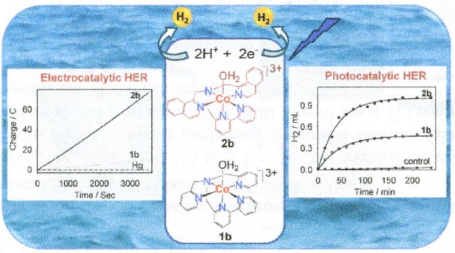

10101 dx.doi.org/10.1021/ic5009472

Quest for Lead Free Relaxors in $YIn_{1-x}Fe_xO_3$ ($0.0 \le x \le 1.0$) System: Role of Synthesis and Structure

Rakesh Shukla, Farheen N. Sayed, Vinita Grover,* Sudhanshu K. Deshpande, Apurav Guleria, and Avesh K. Tyagi*

The $YIn_{1-x}Fe_xO_3$ series was subjected to structural and electrical investigations. The phase relations showed rich crystal chemistry, and phases like C-type, hexagonal, and orthorhombic modifications were observed as a function of temperature. The distortion in BO_5 polyhedra subtly altered YO_7 polyhedra introducing relaxor ferroelectric like behavior in $YIn_{0.7}Fe_{0.3}O_3$.

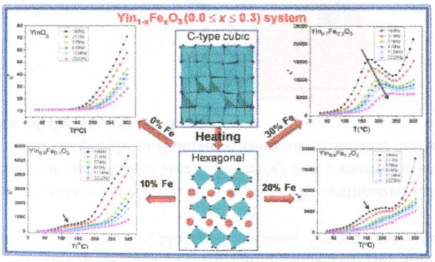

10112 Ⓢ dx.doi.org/10.1021/ic5009736

Triazolyl–Based Copper–Molybdate Hybrids: From Composition Space Diagram to Magnetism and Catalytic Performance

Ganna A. Senchyk, Andrey B. Lysenko,* Artem A. Babaryk, Eduard B. Rusanov, Harald Krautscheid, Patrícia Neves, Anabela A. Valente, Isabel S. Gonçalves, Karl W. Krämer, Shi-Xia Liu,* Silvio Decurtins, and Konstantin V. Domasevitch

The composition space diagram offers intriguing possibilities for the investigation of copper–molybdate hybrid solids. The multicomponent Cu^{II}/ Mo^{VI}-oxide/1,3-bis(1,2,4-triazol-4-yl)adamantane system was thoroughly studied employing the concept and led to three layered copper–molybdate coordination solids. This allowed us to elucidate the relationship between initial reagent concentration/stoichiometry and the stability of the resultant structural motifs. The compounds show catalytic activity in the epoxidation of *cis*-cyclooctene and in the oxidation of benzyl alcohol with different oxidants.

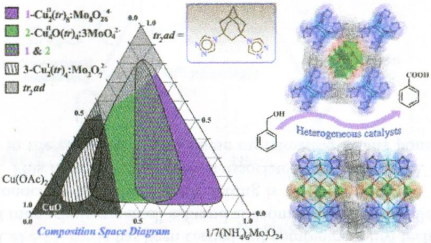

10122 dx.doi.org/10.1021/ic5010352

Immobilization of Ultrafine Bimetallic Ni–Pt Nanoparticles Inside the Pores of Metal–Organic Frameworks as Efficient Catalysts for Dehydrogenation of Alkaline Solution of Hydrazine

Nan Cao, Lan Yang, Hongmei Dai, Teng Liu, Jun Su, Xiaojun Wu, Wei Luo,* and Gongzhen Cheng

Ultrafine bimetallic Ni–Pt nanoparticles immobilized on the MIL-101 exerted high catalytic activity, selectivity, and durability toward hydrogen generation from hydrazine in alkaline solution.

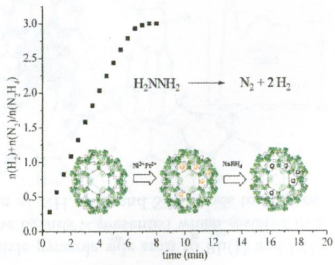

10129 S dx.doi.org/10.1021/ic501067p

Room-Temperature Synthesis of Iron-Doped Anatase TiO_2 for Lithium-Ion Batteries and Photocatalysis

Christian Andriamiadamanana, Christel Laberty-Robert, Moulay T. Sougrati, Sandra Casale, Carine Davoisne, Snehangshu Patra, and Frédéric Sauvage*

Iron-doped nanocrystalline particles of anatase TiO_2 have been successfully synthesized using a complete room-temperature synthetic approach, leading to particles of high surface area (280 m^2/g) and a narrowed band gap of 2.3 eV. These particles were introduced for photocatalysis under white light in standard conditions (AM1.5G) and in lithium-ion batteries to reveal in these two aspects the pros and cons of the doping effect.

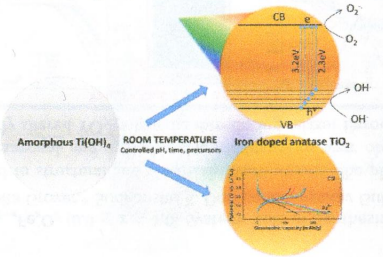

10140 S dx.doi.org/10.1021/ic5011242

High Temperature Structural Study of Gd-Doped Ceria by Synchrotron X-ray Diffraction (673 K ≤ *T* ≤ 1073 K)

Cristina Artini,* Marcella Pani, Andrea Lausi, Roberto Masini, and Giorgio A. Costa

The structural study of the $(Ce_{1-x}Gd_x)O_{2-x/2}$ system at 673 K ≤ *T* ≤ 1073 K revealed the existence of a transition at $x \approx 0.2$ from the CeO_2-based solid solution to the CeO_2 matrix containing intergrown microdomains of cubic Gd_2O_3. The trend of the lattice parameter versus Gd content shows a maximum that shifts toward lower Gd content with increasing temperature, due to the linear decrease of the coefficient of thermal expansion for $x > 0.2$.

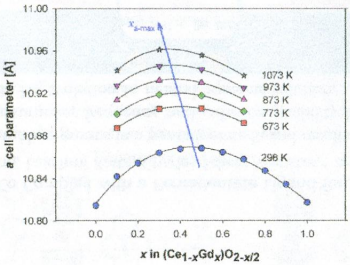

10150 S dx.doi.org/10.1021/ic501112a

Effect of Axial Ligand, Spin State, and Hydrogen Bonding on the Inner-Sphere Reorganization Energies of Functional Models of Cytochrome P450

Sabyasachi Bandyopadhyay, Atanu Rana, Kaustuv Mittra, Subhra Samanta, Kushal Sengupta, and Abhishek Dey*

The inner-sphere reorganization energies of high-spin and low-spin imidazole- and thiolate-bound iron porphyrins are determined to have significant contributions from spin state, axial ligands and hydrogen-bonding interactions to axial ligands.

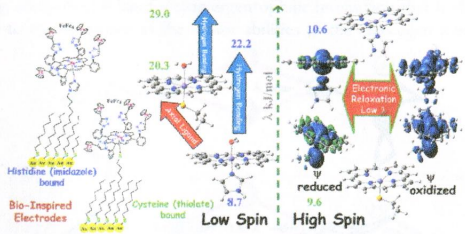

10159 S dx.doi.org/10.1021/ic501158x

Hemilabile and Bimetallic Coordination in Rh and Ir Complexes of NCN Pincer Ligands

Giulia Mancano, Michael J. Page, Mohan Bhadbhade, and Barbara A. Messerle*

The coordination of NCN pincer ligands containing a central NHC donor and labile pyrazole side arms to Rh(I) and Ir(I) resulted in a variety of binding modes. Evidence for hemilabile coordination of the ligands is presented which resulted in a significant impact on the reactivity of these complexes as catalysts for the addition of NH, OH, and SiH bonds to alkynes.

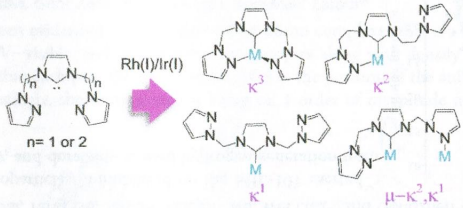

10171 dx.doi.org/10.1021/ic5011456

Structural Transition at 360 K in the $CaFe_5O_7$ Ferrite: Toward a New Charge Ordering Distribution

C. Delacotte, F. Hüe, Y. Bréard, S. Hébert, O. Pérez, V. Caignaert, J. M. Greneche, and D. Pelloquin*

A revisiting structural study of the $CaFe_5O_7$ oxide has been carried out combining TEM techniques and diffraction data. An unexpected monoclinic supercell is found at room temperature while above 360 K a structural change from monoclinic to orthorhombic setting is observed with the disappearing of the superstructure. This reversible transition is associated to a sharp peak in the magnetic susceptibility and a drop in the resistivity curve. These experimental results point out a charge ordering mechanism

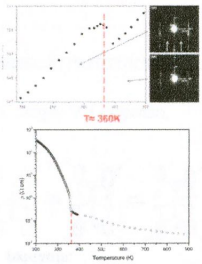

10178 S dx.doi.org/10.1021/ic501152j

Alkali Metal Ion Templated Transition Metal Formate Framework Materials: Synthesis, Crystal Structures, Ion Migration, and Magnetism

Espen Eikeland, Nina Lock, Mette Filsø, Marian Stingaciu, Yanbin Shen, Jacob Overgaard, and Bo Brummerstedt Iversen*

Four formate-based anionic MOFs were synthesized with alkali ions as templating agents using a mild solution chemistry approach. Void space analysis of the crystal structures suggests suitable ion migration channels, but the measured electrochemical response does not corroborate this. In addition the thermal and magnetic properties are reported.

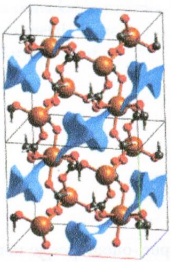

10189 S dx.doi.org/10.1021/ic5011709

Synthesis, Characterization, and X-ray Attenuation Properties of Ultrasmall BiOI Nanoparticles: Toward Renal Clearable Particulate CT Contrast Agents

Murthi S. Kandanapitiye, Min Gao, Joseph Molter, Chris A. Flask,* and Songping D. Huang*

The controlled hydrolysis reaction for producing BiO^+ ions under acidic conditions in the presence of I^- ions and a polymer coating agent leads to the formation of ultrasmall nanoparticles with a narrow size distribution (~2.8 ± 0.5 nm). Such nanoparticles possess very high X-ray attenuation power and can be readily internalized by HeLa cells via endocytosis, suggesting their potential as a cellular X-ray CT contrast agent.

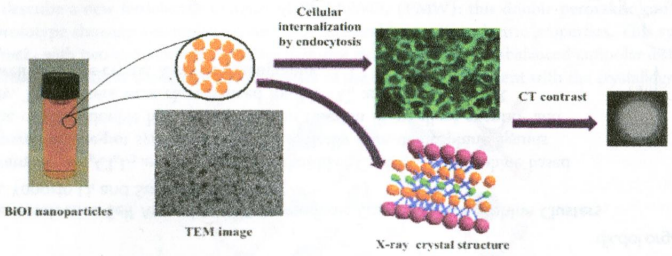

10195 S dx.doi.org/10.1021/ic501181k

Influence of Ligand Flexibility on the Electronic Structure of Oxidized Ni^{III}-Phenoxide Complexes

Minoru Kawai, Takahide Yamaguchi, Shigeyuki Masaoka, Fumito Tani, Takamitsu Kohzuma, Linus Chiang, Tim Storr, Kaoru Mieda, Takashi Ogura, Robert K. Szilagyi, and Yuichi Shimazaki*

The oxidation locus on one-electron-oxidized Ni^{III}-phenoxide complexes with different chelate ring sizes of the dinitrogen chelate backbone was determined by UV–vis–NIR, EPR, resonance Raman, and XAS spectroscopy. The complex $[\mathbf{1}\text{-py}]^{2+}$ with a five-membered chelate backbone was a Ni^{III}-phenoxyl radical, while the six-membered chelate complex $[\mathbf{2}\text{-py}]^{2+}$ could be assigned to the biradical species Ni^{II}-bis(phenoxyl radical) with metal-centered reduction.

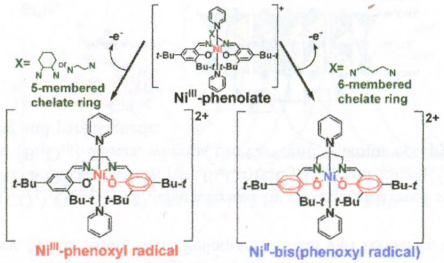

10203 S dx.doi.org/10.1021/ic501222n

Metal and Ligand Effects on Bonding in Group 6 Complexes of Redox-Active Amidodiphenoxides

Leila G. Ranis, Kalpani Werellapatha, Nicholas J. Pietrini, Bruce A. Bunker, and Seth N. Brown*

Molybdenum and tungsten form diamagnetic octahedral complexes with ONO and DOPO ligands containing metal(VI) and two $[L^{cat}]^{3-}$ ligands. In contrast, $Cr(ONO)_2$ in solution and $Cr(DOPO)_2$ form $Cr^{III}(L^{Q})(L^{SQ})$ complexes. Solid $Cr(ONO)_2$ is a singlet, analogous to the Mo and W analogues, but shows much greater charge transfer to the metal via π donation. The covalency of the interaction makes oxidation state assignment problematic, but lends itself to description by a qualitative molecular orbital picture.

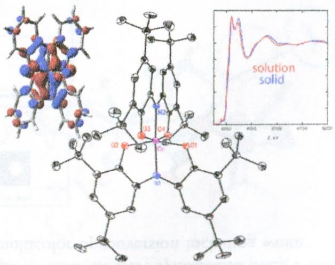

10217 dx.doi.org/10.1021/ic501247x

$[Mn^{III}(Schiff\ Base)]_3[Re^{IV}(CN)_7]$, Highly Anisotropic 3D Coordination Framework: Synthesis, Crystal Structure, Magnetic Investigations, and Theoretical Analysis.

Denis G. Samsonenko, Carley Paulsen,* Elsa Lhotel, Vladimir S. Mironov,* and Kira E. Vostrikova*

A new 3D coordination polymer $[Mn^{III}(acacen)]_3[Re^{IV}(CN)_7]$ was synthesized and characterized. This is the first 3D framework among the compounds composed of homoleptic cyanometallate and $[Mn^{III}(Schiff\ base)]$ complex. Its unusual magnetic behavior results from a interplay of Re–Mn anisotropic spin coupling and ZFS effect of Mn^{III} ions with a noncollinear orientation of the local magnetic axes in the crystal. A theoretical model of anisotropic spin coupling between orbitally degenerate $[Re^{IV}(CN)_7]^{3-}$ anions and Mn^{III} ions is developed.

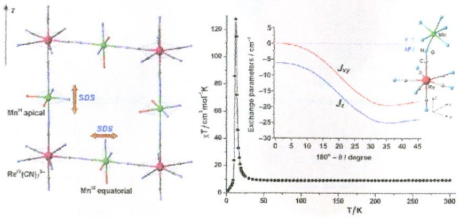

$$\hat{H}_{\text{Re-Mn}} = -J_{xy}(S^x_{\text{Re}}S^x_{\text{Mn}} + S^y_{\text{Re}}S^y_{\text{Mn}}) - J_z S^z_{\text{Re}}S^z_{\text{Mn}}$$

10232 dx.doi.org/10.1021/ic501233w

A One-Pot Diastereoselective Self Assembly of C-Stereogenic Copper(I) Diphosphine Clusters

Xiang-Yuan Yang, Yongxin Li, and Sumod A. Pullarkat*

12-membered "drumlike" $Cu_6Cl_6L_3$ and 8-membered "chairlike" $Cu_4Cl_4L_2$ diphosphine-based clusters were prepared in one-pot syntheses from the optically pure diphosphine ligands synthesized via the catalytic double hydrophosphination reaction in excellent enantio- and diastereoselectivity. The clusters were characterized by ^1H, ^{13}C, and $^{31}P\{^1H\}$ NMR spectroscopy as well as single-crystal X-ray crystallography.

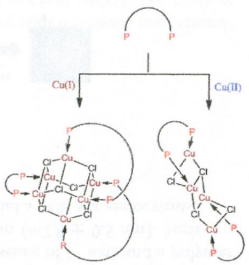

10240 dx.doi.org/10.1021/ic501267f

Synthesis of Terminal Monochalcogenide and Dichalcogenide Complexes of Uranium Using Polychalcogenides, $[E_n]^{2-}$ (E = Te, n = 2; E = Se, n = 4), as Chalcogen Atom Transfer Reagents

Danil E. Smiles, Guang Wu, and Trevor W. Hayton*

Use of the ditelluride complex, $[K(18\text{-crown-}6)]_2[Te_2]$, for chalcogen atom transfer allows for the isolation of both mono- and ditelluride complexes of uranium(IV).

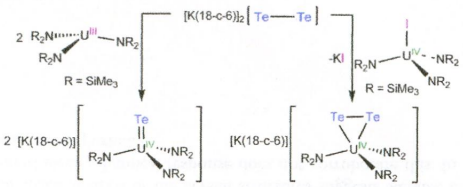

10248 Ⓢ dx.doi.org/10.1021/ic501282d

Surfactant-Thermal Syntheses, Structures, and Magnetic Properties of Mn–Ge–Sulfides/Selenides

Guodong Zhang, Peizhou Li, Junfeng Ding, Yi Liu, Wei-Wei Xiong, Lina Nie, Tom Wu, Yanli Zhao, Alfred Iing Yoong Tok, and Qichun Zhang*

Using hydrazine, ethylenediamine (*en*), 1,2-propanediamine (1,2-*dap*), and 1,3-propanediamine (1,3-*dap*) as structure-directing agents (SDAs) under surfactant (PEG-400) media, four novel crystals $Mn_3Ge_2S_7(NH_3)_4$ (**1**), $[Mn(en)_2(H_2O)]$-$[Mn(en)_2MnGe_3Se_9]$ (**2**), $(1,2\text{-dapH})_2\{[Mn(1,2\text{-dap})_2]Ge_2Se_7\}$ (**3**) and (1,3-dapH)(*puH*)$MnGeSe_4$ (**4**) have been successfully prepared. The structural analysis shows that different SDAs can result in diverse metal coordination geometries or aggregates including MnS_4N_2 octahedra, MnS_3N tetrahedra, $MnSe_4$ tetrahedra, $MnSe_2N_4$ octahedra, Ge_2Se_7 dimer, and $MnGe_3Se_{10}$ T2 cluster.

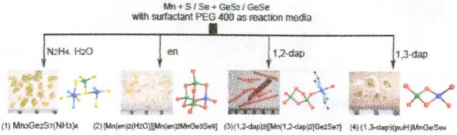

10257 Ⓢ dx.doi.org/10.1021/ic5013022

Novel Fluorite Structured Superparamagnetic $RbGdF_4$ Nanocrystals as Versatile Upconversion Host

Shahzad Ahmad, Rajamani Nagarajan,* Packiya Raj, and G. Vijaya Prakash*

Fluorite structured monodispersed $RbGdF_4$ nanocrystals exhibiting superparamagnetic behavior were synthesized using a wet chemical method. Upon doping with appropriate rare earth ions, they showed multicolor upconversion including white emissions.

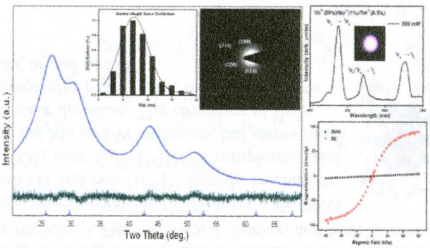

10266 Ⓢ dx.doi.org/10.1021/ic501322w

$Sr_{21}Bi_8Cu_2(CO_3)_2O_{41}$, a Bi^{5+} Oxycarbonate with an Original 10L Structure

Sylvie Malo,* Artem M. Abakumov, Marco Daturi, Denis Pelloquin, Gustaaf Van Tendeloo, Anne Guesdon, and Maryvonne Hervieu

A new oxycarbonate $Sr_{21}Bi_8Cu_2(CO_3)_2O_{41}$ ($Z = 2$), characterized by an original layered structure described as a 10*L*-type structure built up from two structural blocks, namely, $[Sr_{15}Bi_6Cu_2(CO_3)O_{29}]$ and $[Sr_6Bi_2(CO_3)O_{12}]$, was synthesized. In this compound, the Bi^{5+} cations form $[Bi_2O_{10}]$ dimers, whereas the Cu^{2+} and C atoms occupy infinite tunnels running along $\vec{c}$. $Sr_{21}Bi_8Cu_2(CO_3)_2O_{41}$ is insulating and paramagnetic.

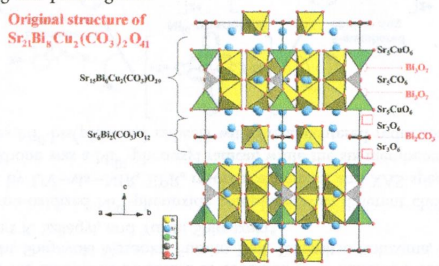

10276 S dx.doi.org/10.1021/ic5013236

The Stability of Mercaptobenzothiazole Based Soft Scorpionate Complexes

Rajeev Rajasekharan-Nair, Dean Moore, Alan R. Kennedy, John Reglinski,* and Mark D. Spicer*

Reaction of 2-mercaptobenzothiazole based soft scorpionate ligands with metal ions results in varying degrees of decomposition. With lower main group metals, loss of a single sulfur atom resulting in formation of a remarkable cationic pentacyclic species is observed, along with expulsion of some of the parent heterocycle. With transition metals there is evidence that in some circumstances the decomposition may be even more catastrophic, resulting in formation of benzothiazole.

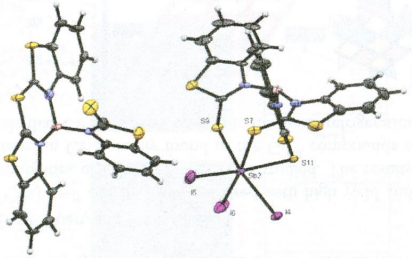

10283 S dx.doi.org/10.1021/ic501328s

Structural and Electric Evidence of Ferrielectric State in Pb_2MnWO_6 Double Perovskite System

Fabio Orlandi,* Lara Righi, Riccardo Cabassi, Davide Delmonte, Chiara Pernechele, Fulvio Bolzoni, Francesco Mezzadri, Massimo Solzi, Marco Merlini, and Gianluca Calestani

In this paper we describe a new ferrielectric compound Pb_2MnWO_6 (PMW): this double perovskite can be considered as a novel structural prototype showing a complex nuclear structure and interesting electric properties. This system crystallizes in the polar group $Pmc2_1$ with two independent lead sites that give rise to a complex unbalanced antipolar distortion. A thorough electrical characterization confirms the ferrielectric character of the system in agreement with the crystallographic observations.

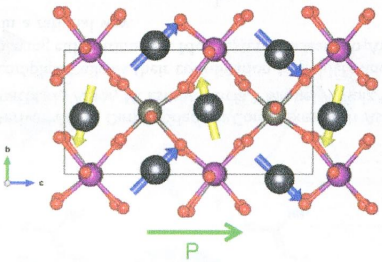

10291 S dx.doi.org/10.1021/ic501330j

Magnetic Relaxation of 1D Coordination Polymers $(X)_2[Mn(acacen)Fe(CN)_6]$, X = Ph_4P^+, Et_4N^+

Michał Rams,* Eugenia V. Peresypkina, Vladimir S. Mironov, Wolfgang Wernsdorfer, and Kira E. Vostrikova*

A simple substitution of cation in 1D polymer, $(cation)_2[Mn^{III}(acacen)Fe^{III}(CN)_6]$, leads to an essential change in magnetic behavior. Due to a pronounced influence of a larger cation Ph_4P^+ on the chain packing in the crystal, the polyanion has a more distorted chain skeleton and, as a consequence, enhanced single chain magnet (SCM) characteristics compared to those for its Et_4N^+ congener.

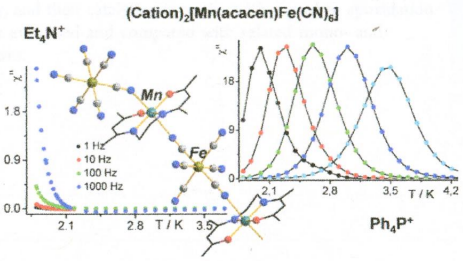

10301 S dx.doi.org/10.1021/ic5013523

Computational Investigation of [FeFe]-Hydrogenase Models: Characterization of Singly and Doubly Protonated Intermediates and Mechanistic Insights

Mioy T. Huynh, Wenguang Wang, Thomas B. Rauchfuss, and Sharon Hammes-Schiffer*

Theoretical calculations in conjunction with supporting experimental data are used to analyze the mechanistic pathway for hydrogen evolution catalyzed by the bioinspired model $Fe_2(adt)(CO)_2(dppv)_2$. This study elucidates the site of reduction and the pK_a values associated with formation of the singly and doubly protonated species, as well as the roles of the ammonium-hydride interaction, flexibility of the bridging CO ligand, and intramolecular electron transfer between the Fe centers in the catalytic cycle for H_2 production.

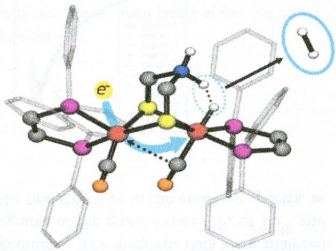

10312 dx.doi.org/10.1021/ic501333s

Zinc(II)-Mediated Nitrile–Amidoxime Coupling Gives New Insights into H^+-Assisted Generation of 1,2,4-Oxadiazoles

Dmitrii S. Bolotin, Kirill I. Kulish, Nadezhda A. Bokach,* Galina L. Starova, Vladislav V. Gurzhiy, and Vadim Yu. Kukushkin*

1,2,4-Oxadiazoles represent an important class of five-membered heterocycles, and their versatile chemistry has been repeatedly reviewed over the years. Zinc(II)-mediated nitrile–amidoxime coupling gives new insights into H^+-assisted generation of 1,2,4-oxadiazoles. All intermediates of the Zn^{II}/H^+-assisted generation of 1,2,4-oxadiazoles were isolated and identified. Zn^{II}-mediated coupling between RCN and amidoximes gives chelates {imidoylamidoxime}Zn^{II}, which rapidly liberate iminium salt in the presence of strong acid, viz. *p*-TolSO_3H. The iminium salts transform to 1,2,4-oxadiazoles in the range from 20 to 65 °C.

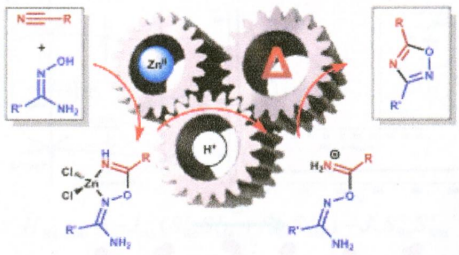

10325 dx.doi.org/10.1021/ic501376v

Gold(I) and Related Heterometallic Derivatives of Dimolybdenum Complexes with Asymmetric Phosphinidene Bridges

Belén Alvarez, M. Angeles Alvarez, Inmaculada Amor, M. Esther García,* Miguel A. Ruiz,* and Jaime Suárez

Multiple Mo–P bonding in the title complexes allows their coordination to gold(I) and related complexes to yield phosphinidene-bridged derivatives displaying either trinuclear Mo_2Au, tetranuclear Mo_3Au, or pentanuclear Mo_4M metal cores (M = Au, Ag, Cu; L = η^6-$C_6H_3{}^tBu_3$) in a rational way.

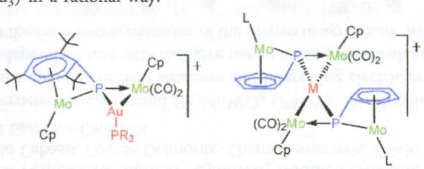

10340 dx.doi.org/10.1021/ic501395p

Lanthanide Coordination Polymers with "fsy-type" Topology Based on 4,4′-Azobenzoic Acid: Syntheses, Crystal Structures, and Magnetic Properties

Shaowei Zhang, Wei Shi,* Leilei Li, Eryue Duan, and Peng Cheng*

Lanthanide coordination polymers (CPs) **1**–**7** can be easily prepared with high yield and possess high thermal stability. Variable-temperature magnetic susceptibilities of CPs **1**–**7** have been studied. The results indicate unusual ferromagnetic couplings between adjacent Gd^{III} cations in CP **3**, rarely found in the Gd^{III} compounds only bridged by $\mu_{1,3}$-COO groups. Meanwhile, the magnetic study reveals that CP **3** displays cryogenic magnetic refrigeration property and CP **5** exhibits slow magnetic relaxation.

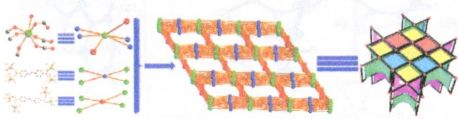

10347 Ⓢ dx.doi.org/10.1021/ic501362b

High-Throughput ab Initio Screening for Two-Dimensional Electride Materials

Tomofumi Tada,* Seiji Takemoto, Satoru Matsuishi, and Hideo Hosono

High-throughput ab initio screening of approximately 34000 materials in the Materials Project was conducted to identify two-dimensional (2D) electride materials, which are composed of ionic layers and anionic electrons confined in a 2D empty space. The screening found that (1) K_2Cl, K_2Br, Rb_2Cl, and Rb_2Br dialkali halides are highly plausible candidates, (2) Li_2F and Na_2Cl dialkali halides are highly challenging candidates, and (3) Sr_2N and Ba_2N nitrides, Y_2C carbide, and $Cs_2O_{1-x}F_x$ dialkali oxide are promising candidates.

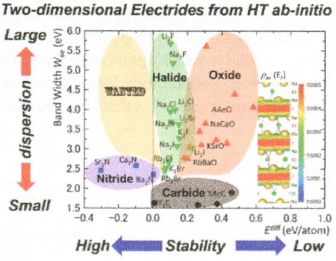

10359 Ⓢ dx.doi.org/10.1021/ic501453h

Crystal Field Splitting of the Ground State of Terbium(III) and Dysprosium(III) Complexes with a Triimidazolyl Tripod Ligand and an Acetate Determined by Magnetic Analysis and Luminescence

Seira Shintoyo, Keishiro Murakami, Takeshi Fujinami, Naohide Matsumoto, Naotaka Mochida, Takayuki Ishida, Yukinari Sunatsuki, Masayuki Watanabe, Masanobu Tsuchimoto, Jerzy Mrozinski, Cecilia Coletti, and Nazzareno Re*

The mononuclear Tb^{III} and Dy^{III} complexes $[Ln^{III}(H_3L)(OAc)](ClO_4)_2{\cdot}MeOH{\cdot}H_2O$ were synthesized with an N_7 tripodal ligand and a bidentate acetate defining a capped-square-antiprismatic coordination geometry. The magnetic data were analyzed by a spin Hamiltonian including the crystal field on Ln^{III} ions to give the energy diagrams of the ground states $^7F_6$ of Tb^{III} and $^6H_{15/2}$ of Dy^{III}. A good correlation was obtained between the energy diagrams and the fine structure in the emission spectra. ac measurements indicated field-induced SIM.

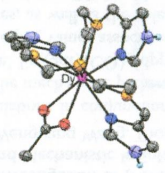

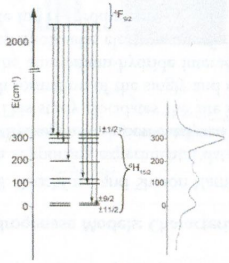

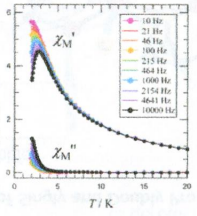

10370 Ⓢ dx.doi.org/10.1021/ic5013796

Modifying Charge and Hydrophilicity of Simple Ru(II) Polypyridyl Complexes Radically Alters Biological Activities: Old Complexes, Surprising New Tricks

Matthew Dickerson, Yang Sun, Brock Howerton, and Edith C. Glazer*

Two Ru(II) polypyridyl complexes with essentially identical photophysical properties but different charges and hydrophilicites were explored as potential agents for photodynamic therapy. Remarkably, the complex carrying a −4 overall charge exhibited excellent light-dependent cytotoxicity while remaining inactive in the dark. In contrast, the complex that was +2 charged caused significant cell death in the absence of the light trigger, likely because of its localization in the mitochondria and destruction of the membrane potential.

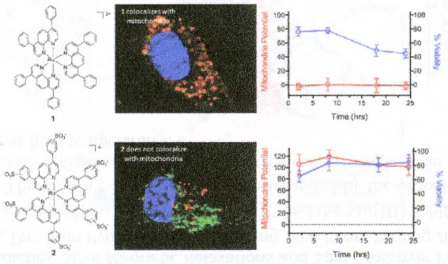

10378 Ⓢ dx.doi.org/10.1021/ic501462y

Study of Iron Dimers Reveals Angular Dependence of Valence-to-Core X-ray Emission Spectra

Christopher J. Pollock, Kyle M. Lancaster, Kenneth D. Finkelstein, and Serena DeBeer*

The sensitivity of valence-to-core X-ray emission spectroscopy (VtC XES) to the Fe−O−Fe bond angle is demonstrated for a series of Fe dimers. The origin of the angular dependence is rationalized using a simple Walsh-type picture for molecular orbital mixing, which has been further verified by DFT calcualtions. The relevance of these findings to the identification of oxygenated intermediates in bioinorganic systems is highlighted, with special emphasis given to the case of soluble methane monooxygenase.

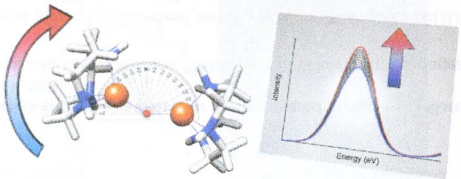

10386 dx.doi.org/10.1021/ic501450f

Increased Eu^{2+} Content and Codoping Mn^{2+} Induced Tunable Full-Color Emitting Phosphor $Ba_{1.55}Ca_{0.45}SiO_4:Eu^{2+},Mn^{2+}$

Shihai Miao, Zhiguo Xia,* Jie Zhang, and Quanlin Liu

A novel single-phased white-light phosphor $Ba_{1.55}Ca_{0.45}SiO_4:Eu^{2+},Mn^{2+}$ was prepared. Increased Eu^{2+} content can produce the blue and green emission centers, and full-color emitting phosphors can be further obtained by codoping with Mn^{2+} to obtain red emission. Energy-transfer efficiency between Eu^{2+} and Mn^{2+} increases and tunable emission can be got with an increase of the Mn^{2+} doping content. Color-tunable $Ba_{1.55}Ca_{0.45}SiO_4:Eu^{2+},Mn^{2+}$ phosphors have great prospects for white light-emitting diodes applications.

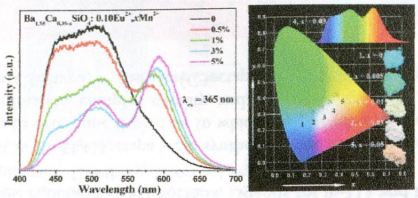

10394 S dx.doi.org/10.1021/ic501483s

Dinuclear Ruthenium Complexes Containing the Hpbl Ligand: Synthesis, Characterization, Linkage Isomerism, and Epoxidation Catalysis

Laia Francàs, Rosa María González-Gil, Daniel Moyano, Jordi Benet-Buchholz, Jordi García-Antón, Lluís Escriche,* Antoni Llobet,* and Xavier Sala*

New dinuclear ruthenium complexes with the hemilabile ligand Hpbl have been prepared and characterized. A number of linkage isomerization processes have been studied and monitored by cyclic voltammetry, and their catalytic properties with regard to epoxidation of *cis*-β-methylstyrene have been evaluated and compared with related mono- and dinuclear Ru–aqua-type complexes.

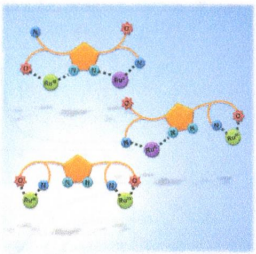

10403 S dx.doi.org/10.1021/ic5014335

Hume–Rothery Phase-Inspired Metal-Rich Molecules: Cluster Expansion of $[Ni(ZnMe)_6(ZnCp^*)_2]$ by Face Capping with $Ni^0(\eta^6$-toluene) and $Ni^I(\eta^5$-Cp*)

Mariusz Molon, Christian Gemel, Paul Jerabek, Lukas Trombach, Gernot Frenking, and Roland A. Fischer*

The synthesis and characterization of three dinuclear Zn-rich complexes of Ni, i.e., $[(\eta^5\text{-Cp}^*)Ni_2(ZnMe)_6(ZnCp^*)(ECp^*)]$ (E = Ga, Zn) and $[(\eta^6\text{-toluene})Ni_2(ZnCp^*)_2(ZnMe)_6]$, are presented, in which the Ni atoms are distributed in a Zn matrix. Two of the complexes are Zn/Ga-substitution isomers and differ only in the nature of one metal atom being either Zn or Ga. Accordingly, one of the two isomers is paramagnetic, and the second isomer is diamagnetic.

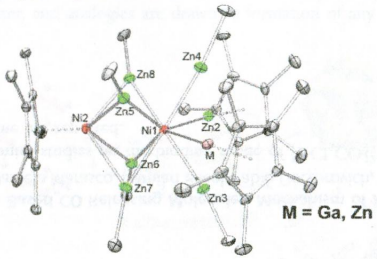

10412 dx.doi.org/10.1021/ic501466z

What a Difference a Carbon Makes: H_4octapa vs H_4C3octapa, Ligands for In-111 and Lu-177 Radiochemistry

Eric W. Price, Brian M. Zeglis, Jacqueline F. Cawthray, Jason S. Lewis,* Michael J. Adam,* and Chris Orvig*

New ligands H_4C3octapa and *p*-SCN-Bn-H_4C3octapa were synthesized and compared to the previously studied ligands H_4octapa and *p*-SCN-Bn-H_4octapa to determine the extent to which the addition of a single carbon atom to the backbone of the ligand would affect metal coordination, complex stability, and, ultimately, utility for in vivo radiopharmaceutical applications. It was found that $[In(C3octapa)]^-$ and $[Lu(C3octapa)]^-$ were substantially different from the analogous H_4octapa complexes.

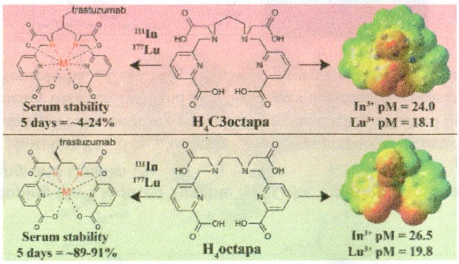

10432 dx.doi.org/10.1021/ic501467w

Enhanced Gas Sorption Properties and Unique Behavior toward Liquid Water in a Pillared-Paddlewheel Metal–Organic Framework Transmetalated with Ni(II)

Olga Karagiaridi, Wojciech Bury, David Fairen-Jimenez, Christopher E. Wilmer, Amy A. Sarjeant, Joseph T. Hupp,* and Omar K. Farha*

Transmetalation of a Zn(II)-based pillared-paddlewheel metal-organic framework to Ni(II) provides the material with permanent and persistent porosity, and endows it with unique reactivity with liquid water.

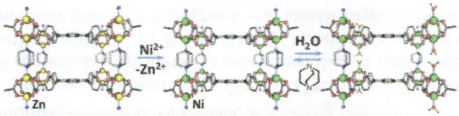

10437 dx.doi.org/10.1021/ic501506s

Synthesis, Crystal Structures, and Magnetic Properties of Cyanide-Bridged W^VMn^{III} Anionic Coordination Polymers Containing Divalent Cationic Moieties: Slow Magnetic Relaxations and Spin Crossover Phenomenon

Jung Hee Yoon, Kwang Soo Lim, Dae Won Ryu, Woo Ram Lee, Sung Won Yoon, Byoung Jin Suh, and Chang Seop Hong*

Trimetallic complexes were prepared by self-assembly of $[W(CN)_8]^{3-}$ and the Mn(III) Schiff base, followed by the addition of a Zn(II) or Fe(II) cationic unit. The W^VMn^{III} anionic chains were separated by the cationic moieties, which causes the slow magnetization relaxation. The Fe(II)-containing compound showed a distinct single-chain magnet behavior at low temperatures and spin crossover at high temperatures.

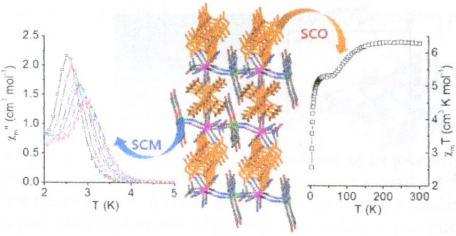

10443 dx.doi.org/10.1021/ic501512p

Single-Source-Precursor Synthesis of Hafnium-Containing Ultrahigh-Temperature Ceramic Nanocomposites (UHTC-NCs)
Jia Yuan, Stefania Hapis, Hergen Breitzke, Yeping Xu, Claudia Fasel, Hans-Joachim Kleebe, Gerd Buntkowsky, Ralf Riedel, and Emanuel Ionescu*

Amorphous SiHfBCN ceramics were prepared from a suitable single-source precursor. Annealing experiments of the SiHfBCN samples in an inert gas atmosphere at temperatures of 1300−1700 °C led to their conversion nanostructured UHTC-NCs, such as $HfC/HfB_2/SiC$ nanocomposites (in argon) and $HfN/Si_3N_4/SiBCN$ nanocomposites (in nitrogen), thus revealing a convenient preparative approach to nanostructured ultrahigh-temperature stable materials starting from a greatly flexible single-source precursor.

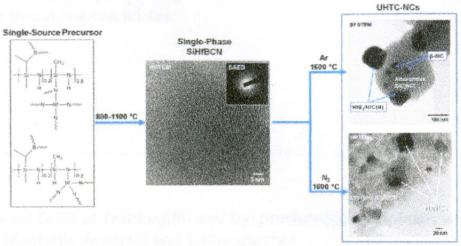

10456 Ⓢ dx.doi.org/10.1021/ic501498g

Interaction between Proteins and Ir Based CO Releasing Molecules: Mechanism of Adduct Formation and CO Release
Ariel A. Petruk, Alessandro Vergara, Daniela Marasco, Damian Bikiel, Fabio Doctorovich, Dario A. Estrin, and Antonello Merlino*

Crystallographic and molecular dynamics studies on the binding mode of $[IrCl_5CO]^{2-}$ to the model protein hen egg white lysozyme are reported.

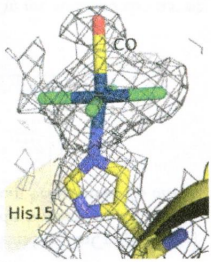

10463 dx.doi.org/10.1021/ic501487c

Magnetic and Thermodynamic Properties of Nanosized Zn Ferrite with Normal Spinal Structure Synthesized Using a Facile Method

Yunong Zhang, Quan Shi,* Jacob Schliesser, Brian F. Woodfield, and Zhaodong Nan*

Normal spinel zinc ferrite ($ZnFe_2O_4$) nanoparticles (NPs) with zero net magnetization were synthesized by a facile coprecipitation method. The heat capacity of the $ZnFe_2O_4$ NPs synthesized using DIPA was measured using a physical property measurement system (PPMS) in the temperature range from 2 to 300 K, and the thermodynamic functions were calculated based on the curve fitting of the experimental heat capacity data.

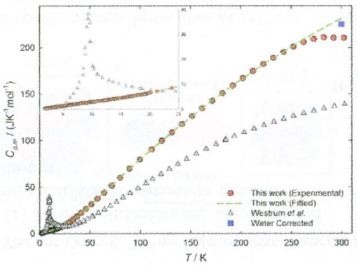

10471 (S) dx.doi.org/10.1021/ic501515c

Influence of Crown Thioether Ligands in the Structures and of Perhalophenyl Groups in the Optical Properties of Complexes with Argentoaurophilic Interactions

Alexander J. Blake, Rocío Donamaría, Vito Lippolis,* José M. López-de-Luzuriaga,* Elena Manso, Miguel Monge, and M. Elena Olmos*

Heteronuclear luminescent Au^I/Ag^I compounds of the types $[\{Au(C_6X_5)_2\}Ag(L)_x]$ (L = crown thioether; X = Cl, F; x = 2, 1, 0.5) were synthesized and structurally characterized showing argentoaurophilic contacts. Their photophysical properties, dependent on the aryl groups, were studied experimentally and theoretically.

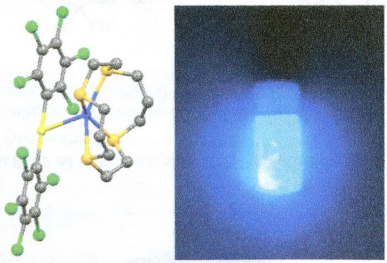

10485 (S) dx.doi.org/10.1021/ic501544d

Di-, Tri-, and Tetranuclear Copper(I) Complexes of Phenanthroline-Linked Dicarbene Ligands

Bo Liu, Shanfei Pan, Bin Liu, and Wanzhi Chen*

Di-, tri-, and tetranuclear Cu(I) complexes of phenanthroline-linked dicarbene ligands were prepared through simple reactions of copper powder and corresponding imidazoliums at room temperature.

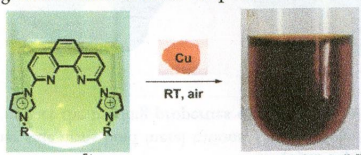

10498 S dx.doi.org/10.1021/ic501573p

Four 2D "Fully Reduced" Polyoxovanadates: Vanadium Oxide Clusters Encapsulating Different Guest Molecules

Hongxiang Wan, Congling Wang, Yu Zhang, Hao Miao, Shuai Zhou, and Yan Xu*

Four 2D fully reduced polyoxovanadates constructed from $[V^{III}_3V^{IV}_{18}P_6O_{60}(DAP)_3]^{9-}$ cages were synthesized. The $[V^{III}_3V^{IV}_{18}P_6O_{60}(DAP)_3]^{9-}$ cages can catch different guest molecules and be connected by Co^{2+} or Cd^{2+} cations to form a wavelike 2D grid structure. Magnetic susceptibility measurement of four compounds indicates ferrimagnetic interactions between vanadium ions.

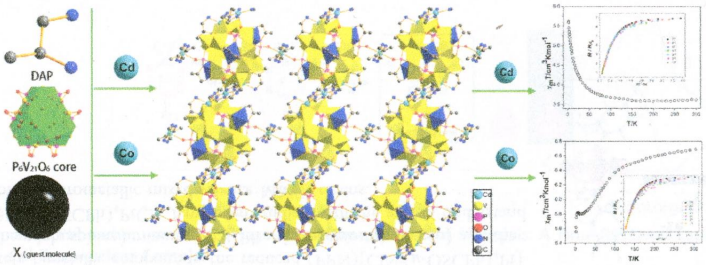

10506 S dx.doi.org/10.1021/ic501587g

Elucidating Self-Assembly Mechanisms of Uranyl–Peroxide Capsules from Monomers

Zuolei Liao, Tapash Deb, and May Nyman*

The mechanism of self-assembly of uranyl peroxide nanocapsules from monomeric precursors is unveiled using formation of the U_{24} capsule, $[UO_2(O_2)(OH)]_{24}^{24-}$, as a model study. Surprisingly, the monomers persist indefinitely until a catalyst is added, and excess peroxide can completely reverse the reaction. The chemistry we have learned here can be applied to assembly of any uranyl peroxide cluster, and analogies are drawn to formation of any metal–oxo cluster, nanoparticle, or material in water.

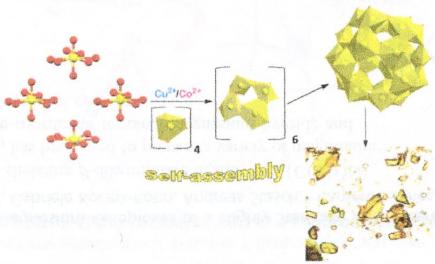

10514 S dx.doi.org/10.1021/ic501590a

Tetra-Armed Cyclen Bearing Two Benzo-15-Crown-5 Ethers in the Side Arms

Mari Ikeda, Mikako Matsumoto, Shunsuke Kuwahara, and Yoichi Habata*

A tetra-armed cyclen bearing two benzo-15-crown-5 ethers in side arms (**1**) is reported. **1** behaves like an argentivorous molecule even though the crown ether side arms bind metal cations. Dynamic conformational changes of the aromatic side arms by forming the **1**·Ag^+ complex impact the binding properties of the crown ethers in the side arms toward alkali metal cations.

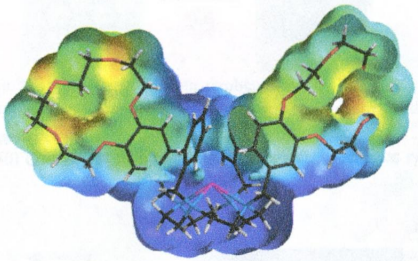

10520 S dx.doi.org/10.1021/ic501595f

Synthesis, Structure, and Catalytic Activity of Pd(II) Complex of Calixoxasmaragdyrin

Tamal Chatterjee and Mangalampalli Ravikanth*

A stable Pd(II) complex of calixoxasmaragdyrin is synthesized, and the crystal structure showed that the calixoxasmaragdyrin macrocycle is highly distorted. The complex exhibited good catalytic activity in the Suzuki–Miyaura cross-coupling reactions.

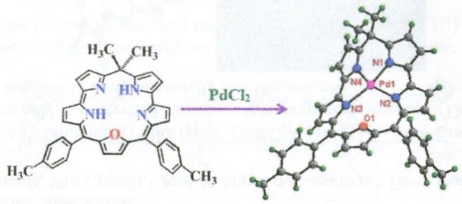

10527 S dx.doi.org/10.1021/ic501623f

Chemistry of Diruthenium Analogue of Pentaborane(9) With Heterocumulenes: Toward Novel Trimetallic Cubane-Type Clusters

R. S. Anju, Koushik Saha, Bijan Mondal, Vincent Dorcet, Thierry Roisnel, Jean-Francois Halet, and Sundargopal Ghosh*

Diruthenium analogue of pentaborane(11) having a dithioformato ligand reacted with $[Mn_2(CO)_{10}]$ under thermolytic and photolytic conditions to generate unprecedented trimetallic cubane-type clusters.

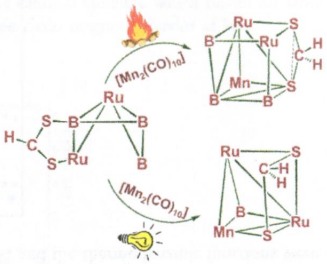

10536 S dx.doi.org/10.1021/ic501585a

Tuning the Photophysical and Redox Properties of Metallocorroles by Iodination

Jenya Vestfrid, Israel Goldberg,* and Zeev Gross*

Selective iodination of aluminum and gallium corroles leads to complexes that display prompt fluorescence, phosphorescence, and delayed thermal fluorescence, all at room temperature.

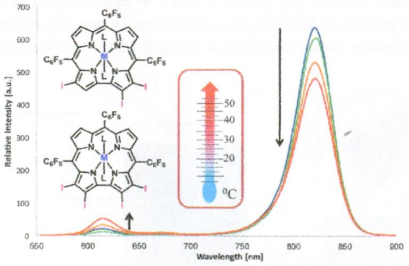

10543 S dx.doi.org/10.1021/ic501638v

Mononuclear Three-Coordinate Magnesium Complexes of a Highly Sterically Encumbered β-Diketiminate Ligand

Merle Arrowsmith, Brant Maitland, Gabriele Kociok-Köhn, Andreas Stasch,* Cameron Jones,* and Michael S. Hill*

The highly sterically encumbered chelating β-diketiminate ligand, $[HC\{C(Me)N\text{-}(2,6\text{-}CHPh_2\text{-}4\text{-}MeC_6H_2)\}_2]^-$, $^{Ar}L^-$, has been used to prepare a variety of magnesium complexes including the first three-coordinate terminal magnesium hydride and some unusually air-stable magnesium alkyl complexes.

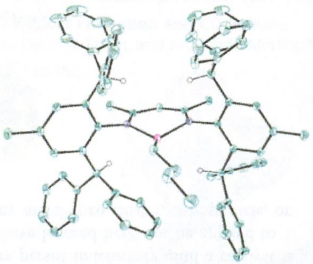

10553 S dx.doi.org/10.1021/ic501659x

On the Road to MM′X Polymers: Redox Properties of Heterometallic Ni···Pt Paddlewheel Complexes

Marcello Gennari, Gonzalo Givaja, Oscar Castillo, Laura Hermosilla, Carlos J. Gómez-García, Carole Duboc, Agustí Lledós, Ruben Mas-Ballesté,* and Felix Zamora*

Two stable discrete bimetallic compounds, the reduced $(PPN)[ClNi(\mu\text{-}OSCPh)_4Pt]$ (PPN = bis(triphenylphosphine)iminium; OSCPh = benzothiocarboxylato) and the oxidized $[(H_2O)Ni(\mu\text{-}OSCPh)_4PtCl]$, have been studied with the aim to understand the process to form heterometallic mixed-valence MM′X chains.

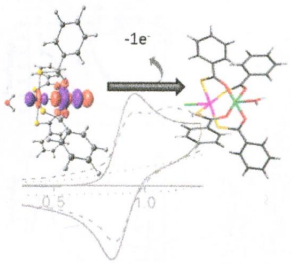

10563 S dx.doi.org/10.1021/ic501665c

Valence Transitions in Negative Thermal Expansion Material $SrCu_3Fe_4O_{12}$

Ikuya Yamada,* Kentaro Shiro, Hidenobu Etani, Shohei Marukawa, Naoaki Hayashi, Masaichiro Mizumaki, Yoshihiro Kusano, Shigenori Ueda, Hideki Abe, and Tetsuo Irifune

The valence states of a negative thermal expansion material, $SrCu_3Fe_4O_{12}$, are investigated by X-ray absorption and ^{57}Fe Mössbauer spectroscopy. Spectroscopic analyses reveal that the appropriate ionic model at room temperature is $Sr^{2+}Cu^{\sim 2.8+}{}_3Fe^{\sim 3.4+}{}_4O_{12}$. The valence states continuously transform to $Sr^{2+}Cu^{\sim 2.8+}{}_3Fe^{\sim 3.4+}{}_4O_{12}$, followed by charge disproportionation into $Sr^{2+}Cu^{\sim 2.8+}{}_3Fe^{3+}{}_{\sim 3.2}Fe^{5+}{}_{\sim 0.8}O_{12}$ upon cooling. The unusual electronic phase transitions in $SrCu_3Fe_4O_{12}$ can be distinguished from the first-order charge-transfer phase transition ($3Cu^{2+} + 4Fe^{3.75+} \rightarrow 3Cu^{3+} + 4Fe^{3+}$) in rare-earth analogues, $RCu_3Fe_4O_{12}$.

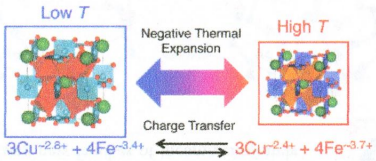

10570 S dx.doi.org/10.1021/ic5016252

Hydrothermal Crystal Growth and Structure Determination of Double Hydroxides $LiSb(OH)_6$, $BaSn(OH)_6$, and $SrSn(OH)_6$

Hiroshi Mizoguchi, Nattamai S. P. Bhuvanesh, Young-Il Kim, Satoshi Ohara, and Patrick M. Woodward*

The crystal structures of $LiSb(OH)_6$, $BaSn(OH)_6$, and $SrSn(OH)_6$ were determined. $LiSb(OH)_6$ has trigonal symmetry and contains alternating $[Li_2Sb(OH)_6]^+$ and $[Sb(OH)_6]^-$ layers. $BaSn(OH)_6$ and $SrSn(OH)_6$ crystallize with a monoclinic structure that possesses a CsCl-type packing of Ba^{2+}/Sr^{2+} cations and $[Sn(OH)_6]^{2-}$ anions. The factors that favor formation of these hitherto unknown crystal structures are discussed using a structure map that compares the structures of various binary and ternary metal hydroxides.

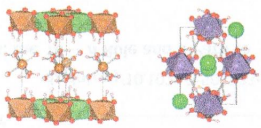

10578 S dx.doi.org/10.1021/ic501677k

Carbene Rearrangements in Three-Coordinate N-Heterocyclic Carbene Complexes of Cobalt(II) Bis(trimethylsilyl)amide

Benjamin M. Day, Kuntal Pal, Thomas Pugh, Jessica Tuck, and Richard A. Layfield*

The cobalt(II) N-heterocyclic carbene (NHC) complexes $[(NHC)Co\{N(SiMe_3)_2\}_2]$, where NHC = IPr, IMes, I^tBu, are reported. Upon heating, the NHC in $[(IPr)Co\{N(SiMe_3)_2\}_2]$ rearranges to the corresponding abnormal (or mesoionic) bonding mode in quantitative yield, giving $[(aIPr)Co\{N(SiMe_3)_2\}_2]$. In contrast, $[(IMes)Co\{N(SiMe_3)_2\}_2]$ is stable with respect to the normal-to-abnormal rearrangement. Refluxing $[(I^tBu)Co\{N(SiMe_3)_2\}_2]$ in toluene results in activation of a *tert*-butyl substituent, which is eliminated as isobutene, followed by formation of the 1-*tert*-butylimidazole complex $[(^tBuIm)Co\{N(SiMe_3)_2\}_2]$.

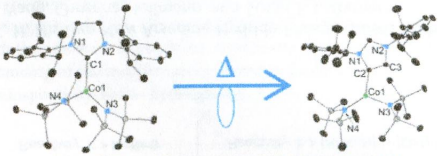

normal-to-abnormal rearrangement

10585 S dx.doi.org/10.1021/ic5016912

Substituent-Dependent Optical and Electrochemical Properties of Triarylformazanate Boron Difluoride Complexes

Stephanie M. Barbon, Jacquelyn T. Price, Pauline A. Reinkeluers, and Joe B. Gilroy*

The straightforward synthesis and detailed characterization of nine substituted triarylformazanate boron difluoride complexes is reported. The complexes were reversibly reduced in two steps electrochemically to their radical anion and dianion forms and exhibited substituent-dependent absorption and emission properties, including significant Stokes shifts. Breaking the symmetry in three different complexes resulted in a modest increase in emission intensity relative to symmetrically substituted derivatives.

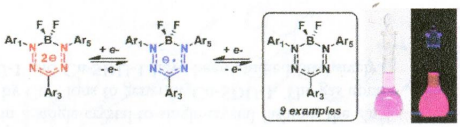

10594 S dx.doi.org/10.1021/ic501696y

Shedding Light on the Photochemistry of Coinage-Metal Phosphorescent Materials: A Time-Resolved Laue Diffraction Study of an Ag^{I}–Cu^{I} Tetranuclear Complex

Katarzyna N. Jarzembska,* Radosław Kamiński, Bertrand Fournier, Elżbieta Trzop, Jesse D. Sokolow, Robert Henning, Yang Chen, and Philip Coppens*

The structure of the triplet excited state of a new crystalline form of a tetranuclear coordination d^{10}–d^{10}-type complex, containing Ag^{I} and Cu^{I} metal centers, has been determined using the Laue pump–probe synchrotron technique. The results show a pronounced shortening of metal–metal contacts in the complex and a considerable strengthening of the argentophilic interaction on excitation.

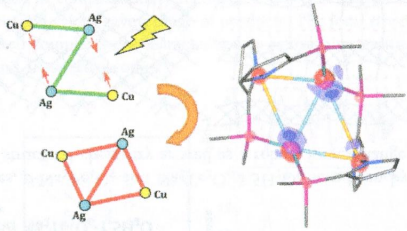

10602 S dx.doi.org/10.1021/ic5017142

Peptide Coupling between Amino Acids and the Carboxylic Acid of a Functionalized Chlorido-gold(I)-phosphane

Margit Kriechbaum, Manuela List, Markus Himmelsbach, Günther J. Redhammer, and Uwe Monkowius*

A protocol for the direct coupling between amino acids and the chlorido-gold(I)-phosphane (p-HOOC(C_6H_4)PPh_2)AuCl has been developed. By applying the EDC·HCl/NHS strategy (EDC·HCl = N-ethyl-N'-(3-(dimethylamino)propyl)carbodiimide hydrochloride, NHS = N-hydroxysuccinimide), the methyl esters of L-phenylalanine, glycine, L-leucine, L-alanine, and L-methionine are coupled with the carboxylic acid of the gold complex in moderate to good yields (62–88%). The molecular structure of the leucine derivative was determined by single-crystal X-ray diffraction.

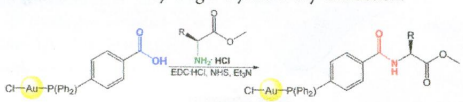

10611 dx.doi.org/10.1021/ic501720h

Assembly, Structure, and Reactivity of Cu_4S and Cu_3S Models for the Nitrous Oxide Reductase Active Site, Cu_Z*

Brittany J. Johnson, Sergey V. Lindeman, and Neal P. Mankad*

The properties of bioinspired copper sulfide clusters were tuned using bridging diphosphines.

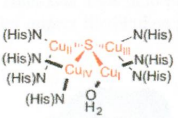

Cu_Z in N_2OR*
Reactivity: $I^- > N{=}N{=}O$

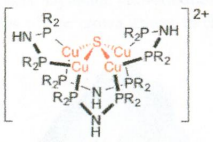

Model complex
Reactivity: $I^- > [N{=}N{=}N]^- > [O{=}N{-}O]^-$

10620 dx.doi.org/10.1021/ic501722d

$LiCa_3As_2H$ and $Ca_{14}As_6X_7$ (X = C, H, N): Two New Arsenide Hydride Phases Grown from Ca/Li Metal Flux

Trevor V. Blankenship, Xiaoping Wang, Christina Hoffmann, and Susan E. Latturner*

Two arsenide hydride phases were synthesized from reactions of arsenic with light-element sources in calcium/lithium metal flux. In both structures, arsenide anions are surrounded by calcium cations; these clusters share edges and corners to form a network that surrounds channels in which the hydride anions reside. Additional light-element anions are incorporated into $Ca_{14}As_6X_7$, where X = H^-, C^{4-}, N^{3-}. Neutron diffraction data were required to distinguish the sites of these anions.

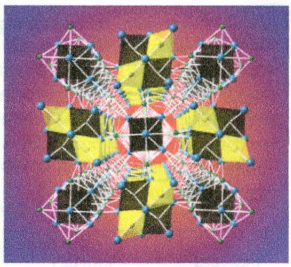

10627 dx.doi.org/10.1021/ic501723n

Orbital Origins of Helices and Magic Electron Counts in the Nowotny Chimney Ladders: the 18 − *n* Rule and a Path to Incommensurability

Vincent J. Yannello and Daniel C. Fredrickson*

The Nowotny chimney ladder (NCL) phases are a family of transition metal main group (T−E) intermetallics remarkable for their double helical motifs and mysterious special stability at valence electron counts corresponding to 14 per T atom. This Article reveals that this 14-electron rule is, in fact, a specific instance of an 18 − *n* rule emerging for T−E intermetallics and describes a strategy suggested by this bonding scheme for synthesizing new families of incommensurately modulated intermetallics.

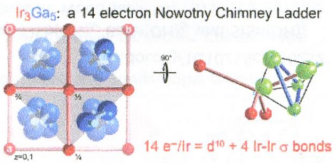

10632 S

dx.doi.org/10.1021/ic501737j

Factors Affecting Hydrogen-Tunneling Contribution in Hydroxylation Reactions Promoted by Oxoiron(IV) Porphyrin π-Cation Radical Complexes

Zhiqi Cong, Haruki Kinemuchi, Takuya Kurahashi, and Hiroshi Fujii*

We examined a kinetic study of benzylic hydroxylation reactions of xanthene and tetralin with oxoiron(IV) porphyrin π-cation radical complex, $(TMP^{+\bullet})Fe^{IV}O(L)$, to investigate the factors controlling the H-tunneling process and succeeded in the observation of nonlinear Arrhenius behavior. The analysis indicates significant contribution of the H-tunneling process, which is controlled by the reaction temperature, the bond dissociation energy of the substrate C–H bond, the reactivity of $(TMP^{+\bullet})Fe^{IV}O(L)$, and probably its Fe=O bond strength.

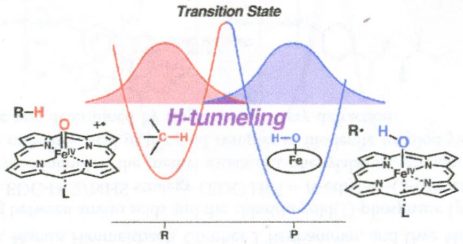

10642 S

dx.doi.org/10.1021/ic501739u

New Polymorphs of Ternary Sodium Tellurium Oxides: Hydrothermal Synthesis, Structure Determination, and Characterization of β-$Na_2Te_4O_9$ and $Na_2Te_2O_6{\cdot}1.5H_2O$

Dong Woo Lee and Kang Min Ok*

Two novel sodium tellurium oxides, β-$Na_2Te_4O_9$ and $Na_2Te_2O_6{\cdot}1.5H_2O$, have been hydrothermally synthesized. The new ternary polymorphs exhibit a rich structural chemistry as well as a robust ion-exchange behavior.

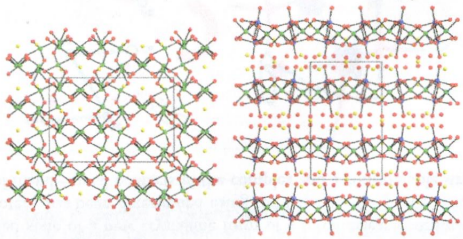

10649 S

dx.doi.org/10.1021/ic5017092

Improving the Porosity and Catalytic Capacity of a Zinc Paddlewheel Metal-Organic Framework (MOF) through Metal-Ion Metathesis in a Single-Crystal-to-Single-Crystal Fashion

Jie Yang, Xiaoqing Wang, Fangna Dai, Liangliang Zhang,* Rongming Wang, and Daofeng Sun*

Through metal-ion metathesis in a single-crystal-to-single-crystal fashion, the Zn^{2+} ions in **SDU-1** were exchanged by Cu^{2+} ions to generate **Cu-SDU-1**. The gas uptake and catalytic properties of **SDU-1** and **Cu-SDU-1** have been studied intensively.

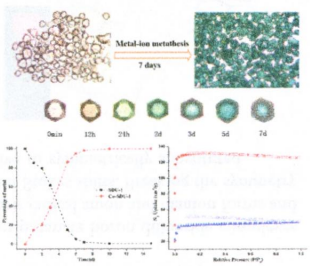

10654 S dx.doi.org/10.1021/ic501715h

Argentophilicity as Essential Driving Force for a Dynamic Cation–Cation Host–Guest System: $[Ag(acetonitrile)_2]^+ \subset [Ag_2(bis\text{-}NHC)_2]^{2+}$ (NHC = N-Heterocyclic Carbene)

Alba Vellé, Andrea Cebollada, Manuel Iglesias, and Pablo J. Sanz Miguel*

An interesting dynamic open-book cationic $[Ag_2(bis\text{-}NHC)_2]^{2+}$ system was found to behave as an excellent host for Ag^+, with argentophilicity being the only "glue" between cations. The ligand-unsupported Ag···Ag interactions found in this system were enough to overcome the inherent electrostatic repulsion between host and guest, stabilizing the system. Furthermore, argentophilic interactions are also observed in solution.

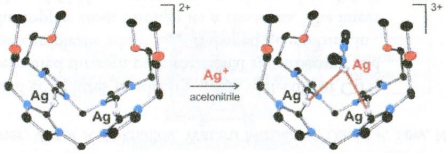

10660 S dx.doi.org/10.1021/ic5017824

A Pentanuclear Lead(II) Complex Based on a Strapped Porphyrin with Three Different Coordination Modes

Stéphane Le Gac,* Eric Furet, Thierry Roisnel, Ismail Hijazi, Jean-François Halet,* and Bernard Boitrel*

Three different coordination modes coexist in a lead(II) strapped porphyrin pentanuclear complex. For the lead cation bound to the strap, X-ray structure analysis and DFT calculations allow a qualitative comparison of the stereochemical activity of the lone pair of lead(II) with two other related complexes.

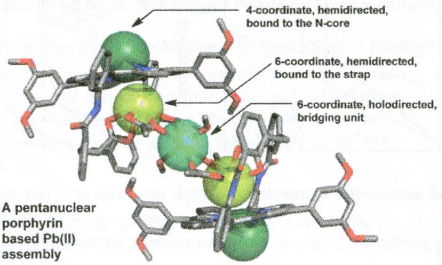

10667 S dx.doi.org/10.1021/ic501815m

Mechanistic Insights into the Catalysis of Electrochemical Proton Reduction by a Diiron Azadithiolate Complex

Marc Bourrez,* Romain Steinmetz, and Frederic Gloaguen*

Through cyclic voltammetry experiments and DFT calculations, a complete mechanism of the catalysis of electrochemical proton reduction by [FeFe]–hydrogenase model, $[Fe_2(\mu\text{-}SCH_2N(H)CH_2S)(CO)_6]$, was established. The proposed mechanism is fully consistent with the observed dependence of the voltammetric responses on the strength of the acid used as a proton source. A better understanding of the mechanism of proton reduction by the biologically relevant model could impact the design of improved catalysts inspired by FeFe–hydrogenase.

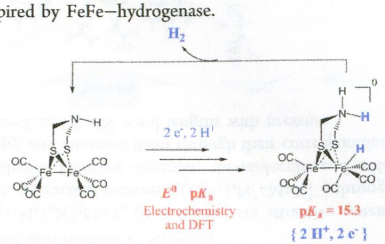

10674 S dx.doi.org/10.1021/ic501821v

Reactions of Alkyne- and Butadiyne-Derived Fluorinated Cyclophosphazenes with Diiron and Dimolybdenum Carbonyls

Dheeraj Kumar, Nem Singh, Anil J. Elias,* Pauline Malik, and Christopher W. Allen*

First reactions of alkyne-derived fluorinated cyclophosphazenes with two different bimetallic metal carbonyls are compared. Reaction with $Fe_2(CO)_9$ resulted in range of products formed by cyclodimerization reactions of the alkynes resulting from cleavage of Fe−Fe bond, whereas reaction with $Cp_2Mo_2(CO)_6$ resulted in simple tetrahedral complexes with retention of Mo−Mo bond. The new iron and molybdenum complexes and cluster compounds showed interesting differences in their spectral and structural properties, and these have been compared.

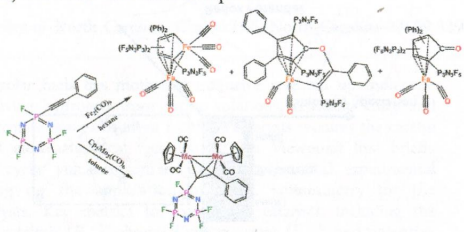

10685 S dx.doi.org/10.1021/ic501818w

Solid-State Structural Studies of Chromium(III) Nicotinato Nutritional Supplements

T. H. Nguyen Pham, Jade B. Aitken, Aviva Levina, and Peter A. Lay*

X-ray absorption spectroscopy and other spectroscopic methods were used to characterize Cr(III) nicotinato nutritional supplements that have long been used in complementary medicine. Different ratios of nicotinic acid and $CrCl_3{\cdot}6H_2O$ (*trans*-$[CrCl_2(OH_2)_4]Cl{\cdot}2H_2O$) at different pH values gave a range of products. The local structures of Cr(III) nicotinato complexes obtained at pH 7 and of the patented complex were characterized by performing multiple-scattering analysis of their EXAFS spectra as well as EPR, UV−vis, and IR spectroscopies.

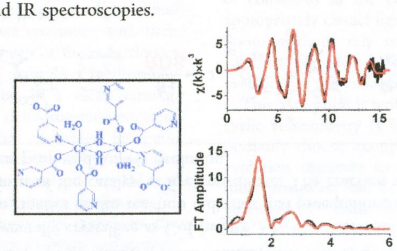

10695 S dx.doi.org/10.1021/ic501852a

Revelation of Varying Coordination Modes and Noninnocence of Deprotonated 2,2′-Bipyridine-3,3′-diol in {Os(bpy)$_2$} Frameworks

Prabir Ghosh, Ritwika Ray, Ankita Das, and Goutam Kumar Lahiri*

Isomeric $\mathbf{1}^+$ and $\mathbf{2}^+$ represent unrecognized N,O$^-$ and usual N,N coordination modes involving O−H···N and O−H···O hydrogen bonding interactions at the back face of monodeprotonated 2,2′-bipyridine-3,3′-diol, respectively. $\mathbf{1}^+$ and $\mathbf{2}^+$ exhibit distinctive structural, electrochemical, spectral, as well as noninnocent features.

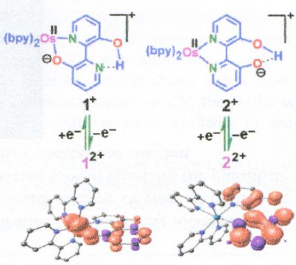

10708 S dx.doi.org/10.1021/ic501854g

Bulk and Molecular Compressibilities of Organic–Inorganic Hybrids $[(CH_3)_4N]_2MnX_4$ (X = Cl, Br); Role of Intermolecular Interactions

Jose Antonio Barreda-Argüeso, Lucie Nataf, Yamilet Rodríguez-Lazcano, Fernando Aguado, Jesús González, Rafael Valiente, Fernando Rodríguez,* Heribert Wilhelm, and Andrew P. Jephcoat

Hybrid inorganic/organic materials $[(CH_3)_4N]_2MnX_4$ (X = Cl, Br) are attractive systems for pressure studies since they are readily compressible through the weak interaction between $[(CH_3)_4N^+/MnX_4^{2-}]$ through hydrogen bonds and contrast with the small compressibility of both tetrahedra. Here we determine the molecular and lattice compressions by X-ray absorption and diffraction and Raman spectroscopy, and compare them through their corresponding equation-of-state. The stretching A_1 mode frequencies provide precise Mn–X and C–N bond lengths with pressure.

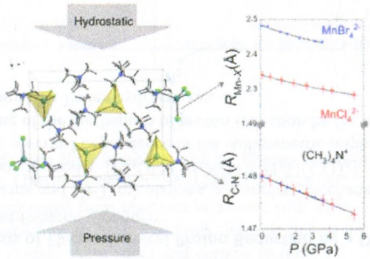

10716 S dx.doi.org/10.1021/ic501906z

A Mononuclear Transition Metal Single-Molecule Magnet in a Nuclear Spin-Free Ligand Environment

Majed S. Fataftah, Joseph M. Zadrozny, Dylan M. Rogers, and Danna E. Freedman*

We discuss the influence of rhombic and axial zero-field splitting on quantum information processing applications and future molecular synthesis.

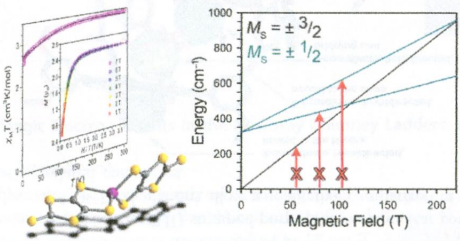

10722 S dx.doi.org/10.1021/ic501899c

Changes in the Geometries of C_2H_2 and C_2H_4 on Coordination to CuCl Revealed by Broadband Rotational Spectroscopy and ab-Initio Calculations

Susanna L. Stephens, Dror M. Bittner, Victor A. Mikhailov, Wataru Mizukami, David P. Tew, Nicholas R. Walker,* and Anthony C. Legon*

The molecular geometries of isolated complexes in which a single molecule of C_2H_4 or C_2H_2 is bound to CuCl are determined through pure rotational spectroscopy and ab-initio calculations. Both of these complexes adopt C_{2v}, T-shaped geometries in which the hydrocarbon binds to the copper atom through its π electrons. The linear and planar geometries of free C_2H_2 and C_2H_4, respectively, are observed to distort significantly on attachment to CuCl, and the changes are quantified precisely.

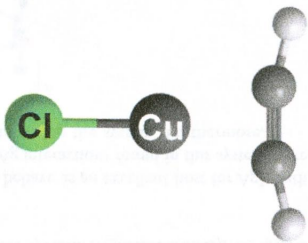

10731 S dx.doi.org/10.1021/ic501961d

Comparative DNA Binding Abilities and Phosphatase-Like Activities of Mono-, Di-, and Trinuclear Ni(II) Complexes: The Influence of Ligand Denticity, Metal–Metal Distance, and Coordinating Solvent/Anion on Kinetics Studies

Vimal K. Bhardwaj* and Ajnesh Singh

The influence of ligand denticity and coordinating solvents/anions on the catalytic activities (DNA binding followed by phosphate ester bond cleavage) was investigated. Complex **3** was found to be active toward catalytic cleavage of phosphate ester bond of DNA model, where binding accompanied by nucleophilic attack of coordinated solvent facilitates the phosphate ester bond cleavage. Complex **3** exhibits 3.86×10^5 times greater rate enhancement than uncatalyzed reaction.

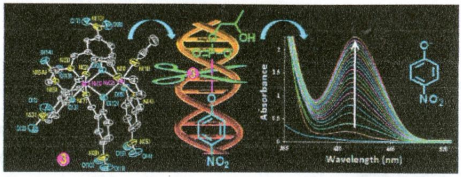

10743 S dx.doi.org/10.1021/ic501975r

Dihydrogen Activation by Cobaloximes with Various Axial Ligands

Gang Li, Deven P. Estes, Jack R. Norton,* Serge Ruccolo, Aaron Sattler, and Wesley Sattler

From donor solvents, cobaloximes generally crystallize as $Co(dmgBF_2)_2L_2$ (L = solvent). In solution these cobaloximes react with H_2 to generate a H• donor. The kinetics of this reaction indicates that preequilibrium dissociation of L precedes reaction with H_2, indicating that the active form of the catalyst is five-coordinate. The reaction with hydrogen is the reverse of the bimolecular mechanism that has been proposed for H_2 evolution.

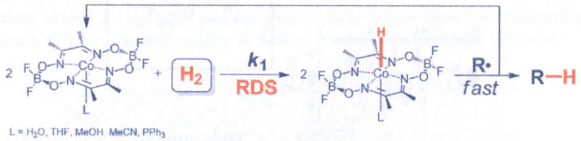

10748 S dx.doi.org/10.1021/ic502005u

Structure–Redox–Relaxivity Relationships for Redox Responsive Manganese-Based Magnetic Resonance Imaging Probes

Eric M. Gale, Shreya Mukherjee, Cynthia Liu, Galen S. Loving, and Peter Caravan*

The Mn(II/III) redox couple represents a potentially powerful mechanism to generate MRI contrast in response to redox dynamics. Ten Mn complexes were synthesized, and the effects of ligand structure and electronics on Mn(II) versus Mn(III) relaxivity, solution structure, stability, solution dynamics, and redox potential were characterized by pH-potentiometry, UV–vis, ^1H and ^{17}O NMR, and cyclic voltammetry. A 7.5-fold relaxivity turn-on was observed upon reduction of Mn(III).

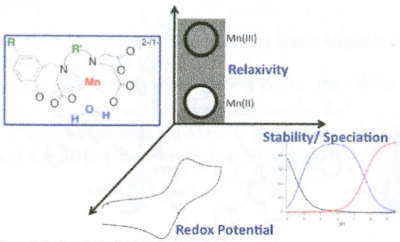

10762 Ⓢ dx.doi.org/10.1021/ic5020412

Structural Plasticity: How Intermetallics Deform Themselves in Response to Chemical Pressure, and the Complex Structures That Result

Veronica M. Berns and Daniel C. Fredrickson*

We propose and explore the concept of structural plasticity, the hypothesis that, like the dislocations underlying the malleability of some metals, the periodic distributions of interfaces in some complex intermetallics emerge in response to stresses—but this time ones inherent in the defect-free parent structure, rather than applied externally. Using DFT-chemical pressure analysis, we show how such stresses arising in the simple $CaCu_5$ type leads to a series of structures, including a Tsai-type quasicrystal approximant.

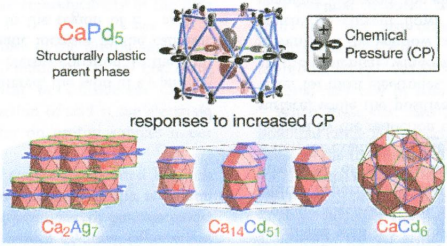

10772 dx.doi.org/10.1021/ic502162p

Impact of Substituents and Nonplanarity on Nickel and Copper Porphyrin Electrochemistry: First Observation of a Cu^{II}/Cu^{III} Reaction in Nonaqueous Media

Yuanyuan Fang, Mathias O. Senge,* Eric Van Caemelbecke, Kevin M. Smith, Craig J. Medforth, Min Zhang, and Karl M. Kadish*

A series of nickel(II) *meso*-tetraalkylporphyrins was electrochemically investigated along with nickel(II) and copper(II) derivatives of dodecaphenylporphyrin and octaethyltetraphenylporphyrin. Each investigated porphyrin exhibits three oxidations, the first two of which are macrocycle-centered to give the porphyrin dication followed by an M^{II}/M^{III} process at more positive potentials.

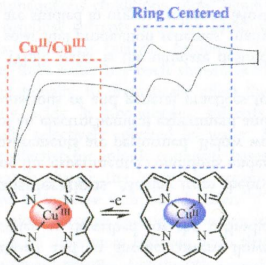

Additions and Corrections

10779 dx.doi.org/10.1021/ic502140y

Correction to van der Waals Radii of Noble Gases

Jürgen Vogt* and Santiago Alvarez*

Ⓢ Supporting Information available via online article